

## Structure of Marangoni-driven singularities

R. Krechetnikov

*Department of Mechanical Engineering, University of California, Santa Barbara, California 93106, USA*

(Received 22 October 2010; accepted 31 January 2012; published online 28 February 2012)

This work presents an analytical study of the structure of steady Marangoni-driven singularities in the context of chemical-reaction driven tip-streaming, which identifies the conditions when such singularities are observable. As motivated by experimental observations of the conical symmetry of the problem, one can construct self-similar solutions of the Stokes equations, which are singular at the tip; these solutions, however, provide no information on the thread structure which is responsible for a resolution of the singularity via tip-streaming. The cone-tip singularity is resolved here with the help of asymptotic matching of the cone and thread solutions using slender jet approximation, which gives an explicit asymptotic formula for the thread radius and thus of the emitted droplets size as a function of physical parameters governing the problem. © 2012 American Institute of Physics. [<http://dx.doi.org/10.1063/1.3685831>]

### I. INTRODUCTION

Formation of singularities at fluid interfaces has always been fascinating and served as an inexhaustible source for many studies. However, a special class of these phenomena—self-driven Marangoni singularities—has not been thoroughly studied as opposed to the singularities forced externally, e.g., with straining or extensional flows. Existence of general Marangoni-driven singularities was recently addressed with mean-curvature flow theory.<sup>1</sup> The present work focuses on the structure of steady self-driven Marangoni singularities: while the analysis and results are general and applicable to Marangoni effects of various origins, the discussion is provided in the context of chemically driven Marangoni flows.

#### A. History of the problem and motivation

The fact that chemically induced Marangoni effects, i.e., fluid flows resulting from variations of interfacial tension, can transfer chemical into mechanical energy directly has been known for a long time, e.g., in the context of camphor scrapings.<sup>2,3</sup> Among the regimes of interfacial mechanical motion are violent and erratic pulsations studied in the works of Garner *et al.*,<sup>4</sup> Haydon,<sup>5</sup> and Lewis;<sup>6</sup> such motions may even lead to localized eruptions.<sup>7</sup> It is this latter circumstance that is of central interest to this work, namely, the formation of interfacial singularities due to Marangoni effects. Historically, these dynamic effects were found to be responsible for the drop oscillations, formation of pointed ends at the drop interface with occurrence of recirculation vortices,<sup>4</sup> and spontaneous emulsification;<sup>5</sup> this is opposed to the earlier “static” understanding that the spontaneous emulsification of oleic acid-paraffin oil mixtures in dilute alkali results from the existence of a negative interfacial tension at the oil-water interface.<sup>8</sup>

As a paradigm, the problem under consideration here is the steady tip-streaming induced by chemical reaction-driven Marangoni effects, which is motivated by the experimental observations of Fernandez and Homsy<sup>9</sup> shown in Figure 1. In the physical problem at hand, a chemical reaction at the interface between the two phases—surrounding more viscous phase 2 (oil + acid) and less viscous phase 1 in the pendant drop (water + alkaline)—produces surfactant. As a possible explanation of the observed phenomena, it was suggested<sup>10</sup> that the surfactant ends up being distributed non-uniformly along the interface in a self-sustained fashion, which drives Marangoni flow in both phases and

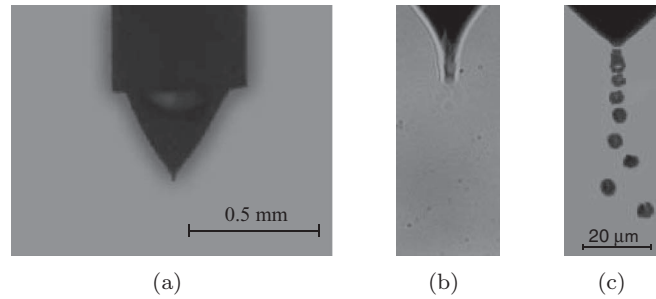


FIG. 1. Steady tip-streaming:<sup>9,10</sup> (a) cone, (b) thread, (c) thread break-up into small droplets.

sweeps surfactant towards the tip of the conical drop. The resulting ultra low interfacial tension in the tip area allows the interface to tear up and to create a thin thread, cf. Figure 1(b), through which the phase 1 is ejected into phase 2, cf. Figure 1(c). The evolution of the thread itself is usually unsteady in view of the process of breaking-up; however, much longer (stable) threads (streamers) were observed in the experiments of Mansfield.<sup>11</sup> It is remarkable that the physical system in Figure 1 demonstrates a substantial separation of scales: the pendant drop is of 0.5 mm diameter, while the thread is about  $5\ \mu\text{m}$  thick, i.e., the tip area appears as a singularity at the scale of the pendant drop, see Figure 1(a). Predicting a scaling for the thread radius, which is *the key question* in the tip-streaming phenomena, was left unanswered in the above mentioned work of Krechetnikov and Homsy.<sup>10</sup> Developing an asymptotic theory for the scaling of the size of the thread and thus of the emitted droplets is the main focus of the present study.

The chemical reaction-driven tip-streaming studied here should be put in the context of general tip-streaming phenomena, which include tip-streaming in externally imposed shear or extensional flows, such as in the four-roll mill device.<sup>12</sup> The basic features of externally driven tip-streaming were quite extensively studied experimentally, see the review by Stone.<sup>13</sup> Starting with experiments by Taylor,<sup>12</sup> it is known that drops with low viscosity relative to the ambient fluid, i.e., with viscosity ratio  $\mu_1/\mu_2 < O(0.1)$ , can lead to the tip-streaming. Later experimental studies by de Bruijn<sup>14</sup> in simple shear flows distinguished two primary modes of drop break-up: (1) a *fracture* mode occurring for pure fluids at a certain shear rate (equivalently, at a critical capillary number  $Ca_c$ ), accompanied by the formation of satellite droplets, and (2) *tip-streaming*, which takes place in the presence of surfactants and produces much smaller drops without satellites. The shear rates required for the last type of break-up in simple shear flows can be two orders of magnitude lower than for the fracture mode. In the case of extensional (straining) flows, the presence of surfactant may also lower significantly the critical capillary number<sup>15,16</sup> from that for pure fluids studied by Acrivos and Lo.<sup>17</sup> While the effect of surfactants appears to lower  $Ca_c$ , the limits of low (dilute) and high (saturated) concentrations of surfactant lead to  $Ca_c$  corresponding to the pure liquid case. The last fact indicates the importance of surfactant gradients in the tip-streaming phenomena as elucidated by de Bruijn<sup>14</sup> for simple shear flows and by Eggleton *et al.*<sup>18,19</sup> for extensional flows. Further discussion of the physical mechanisms behind surfactant effects can be found in the works by Stone<sup>13</sup> in the context of externally driven tip-streaming, Krechetnikov and Homsy<sup>10</sup> in the context of chemical reaction-driven tip-streaming, and Anna and Mayer<sup>20</sup> in the context of flow focusing. Here, however, we will be studying tip-streaming phenomena induced not by externally imposed flows, but driven by a chemical reaction at the interface. Also, while the fluids viscosity ratio  $\mu_1/\mu_2$  in experiments<sup>9</sup> complies with the above mentioned restriction  $\mu_1/\mu_2 < O(0.1)$ , the theory developed here shows the possibility of tip-streaming regardless of the value of  $\mu_1/\mu_2$ .

## B. On the key problem and methodology

While the physical system in Figure 1(a) exhibits a conical symmetry, the singularity associated with that symmetry, i.e., the cone tip, is resolved physically by the tip-streaming phenomena as shown in Figures 1(b) and 1(c). Another possibility, which is realized physically as a time-dependent

solution, is a rounded cone tip. Based on the standard understanding of capillary phenomena, one can formulate *the key problem* as a resolution of the following paradox:

- (I) On one hand, in order to get a conical drop with a pointed end of an infinite curvature one needs the interfacial tension to diverge,  $\sigma \rightarrow \infty$  as  $r \rightarrow 0$ , which follows from the self-similar solution construction in Sec. III and the fact that the Marangoni-induced flow should be directed from the base of the drop towards its tip.
- (II) On the other hand, in order to get the standard externally driven tip-streaming it is necessary that the interfacial tension  $\sigma \rightarrow 0$ ; in the experiments of Fernandez and Homsy,<sup>9</sup> it was also observed that the emitted droplets carry surfactant and thus have low interfacial tension.

Thus, the problem is to reconcile (I) and (II), which should also lead to the prediction of the thread radius. Speaking in general terms of perturbation methods, the phenomena considered here belong to the class of singular as opposed to regular perturbation problems, since the self-similar solution for the conical drop with a singular tip needs to be perturbed to include an asymptotically thin, but finite, thread. This can also be seen from the fact that the base state—the self-similar stream-function solution  $\Psi^0$  with conical symmetry—is singular at the tip  $r = 0$  and thus a construction of a perturbed solution in order to resolve the singularity at  $r = 0$  via regular perturbations,  $\Psi = \Psi^0 + \epsilon\Psi^1 + \dots$  with some small parameter  $\epsilon \ll 1$ , is not possible simply because  $\Psi^1$  cannot cancel  $\Psi^0$  in the neighborhood of the singular point, as  $\Psi^0$  does not depend upon  $\epsilon$  in the regular perturbation scheme. Therefore, application of the domain (boundary) perturbation method,<sup>21,22</sup> which is widely used in interfacial problems with non-singular base states, e.g., flat interfaces<sup>23</sup> and circular drops,<sup>24</sup> is not feasible.

The methods utilized here originate from other singular perturbation problems, e.g., the dip-coating problem of Landau and Levich,<sup>25</sup> where thickness of the thin film deposited in the process of dip-coating is found by matching asymptotically to the static meniscus via a dynamic transition region, in which the viscous and capillary forces balance each other. As will be discussed in Sec. IV, matching procedure in the present problem is justified by the recent results<sup>26</sup> which extend the qualitative and, in certain cases, quantitative validity of lubrication approximations to certain classes of non-unidirectional flows.

Since the motivating system<sup>9</sup> is two-phase with non-equal viscosities, the reduction of the problem to one phase will simplify the analysis considerably. This reduction will be done with the help of the following proposition, the proof of which is given in Appendix A and which was used in a particular form by Layton.<sup>27</sup>

*Proposition 1 (Principle of equivalence of one- and two-phase interfacial motions):* Given a steady motion of a system of two phases with non-equal viscosities,  $\mu_1 \neq \mu_2$ , separated by a dynamic interface in  $\mathbb{R}^2$  (or, in the axisymmetric case, in  $\mathbb{R}^3$ ), where both phases are in the Stokes flow regime and, at least, one of the phases does not contain singularities, one can replace this system with an equivalent one-phase system of viscosity  $\mu' = \mu_1 - \mu_2$  such that the interfacial motion is identical to the original two-phase system. If  $\mu' < 0$ , then the sign of the interfacial tension of the equivalent one phase must be changed.

Therefore, if the outer phase is more viscous, then indeed  $\mu' < 0$ , and the equivalent one-phase system should have negative *effective* surface tension. In this context, it is worth mentioning that the existence of negative *physical* interfacial tension is conjectured in certain physical problems such as electro-capillary phenomena in molten metals, where the metal surface fold into complex fractal corrugations of vast total surface area.<sup>28</sup> However, in the context of the history of emulsification phenomena mentioned earlier, it is likely that the physical interfacial tension is positive and fractal corrugations are due to ultra-low interfacial tension and its variations. In our case, though, the negative interfacial tension is just an intermediate mathematical result, while the interfacial tension in the original two-phase physical system is positive. In addition to the proof of Proposition 1 in Appendix A, it will be illustrated by a direct comparison of one- and two-phase solutions in Sec. III.

### C. Analogous problems

The apparent similarity of the observed cone shape of the drop in the steady tip-streaming regime to Taylor cones<sup>29–32</sup> is remarkable. While both the cone shape and tip-streaming (bursting) effects suggest an analogy to the phenomena of formation of stable cones in electrified liquid interfaces, the underlying physical mechanisms are different.<sup>10</sup> As explained by G. I. Taylor (who assumed equipotentiality of the interface), the conical shape arises as a balance of normal stresses: the electrostatic pressure  $p_E = \epsilon_0 E_n^2/2$  induced by the normal component of electrical field  $E_n$  (the tangential component being zero in view of equipotentiality) equilibrates with the capillary pressure  $p_\sigma = \sigma \cot \alpha/r$  which varies inversely with the distance from cone tip,  $r$ , so that  $E_n \sim (\sigma/\epsilon_0 r)^{1/2}$ . In the case of gradients of the interfacial potential, the tangential component of electrical stresses  $\sim \epsilon_0 E_n E_\tau$  can be either negligible or lead to swirling or nonswirling motion inside the Taylor cone<sup>33</sup> without influencing its self-similar conical shape. In our case, on the other hand, the conical shape is produced as a result of balancing both normal and tangent stresses, and the predominant role is played by the gradient of surface tension balanced by viscous stresses at the interface. As a consequence, the cone shape is due to nontrivial fluid motion both inside (which is analogous to that produced in Taylor cones by tangential stresses) and outside the cone.

The problem of predicting the emitted jet diameter exists in the Taylor cone problem too and, to the author's knowledge, has not been resolved yet.<sup>29,30</sup> The development of the methodology to predict the thread properties in our problem may also provide some insight on how to construct the jet solution in the Taylor cone problem, but this is out of the scope of the present paper.

### D. Paper outline

The paper is organized as follows. The goal of the main body of the paper is to construct a global non-singular solution for Marangoni-driven singularities in the axisymmetric three-dimensional (3D) case formulated in Sec. II. The analysis is comprised of the study of the self-similar structure of the singularity, Sec. III, and the resolution of this singularity via singular perturbation procedure, Sec. IV, which matches the self-similar solution in the cone region to the thread solution. Because of the natural geometries of these two regions, the cone solution is considered in spherical coordinates, Secs. II and III, while the thread solution is constructed in cylindrical coordinates, Sec. IV. The presentation is concluded with the discussion of open questions in Sec. V.

## II. PROBLEM FORMULATION: SPHERICAL COORDINATES

The geometry of the problem is sketched in Figure 2(a). In the mathematical formulation, we will utilize the facts that the phenomena are *steady* and *axisymmetric*, so that the appropriate system of coordinates is either cylindrical or spherical; however, due to the additional conical symmetry of the problem, we choose to work with spherical coordinates,

$$x = r \sin \theta \cos \phi, \quad y = r \sin \theta \sin \phi, \quad z = r \cos \theta, \quad (1)$$

where  $\theta \in [0, \pi]$ ,  $\phi \in [0, 2\pi]$ . The cone semi-angle  $\theta^*$  in Figure 2(a) is dictated by stratification and wetting properties of a syringe needle.<sup>9</sup> Also, in practice, when the conical drop is of finite size, for the phenomenon to be steady there should be some mass flux supplied; the latter condition can be expressed in terms of the mass flow rate  $Q_\infty$  through the thread of radius  $\bar{h}_\infty$ , which is another given parameter in the problem.

Defining interface in terms of  $(r, \theta)$ -variables,  $H(r, \theta) = \theta - h(r)$ , the normal  $\mathbf{n}$  and tangent  $\mathbf{t}$  vectors are given by

$$\mathbf{n} = \frac{\nabla H}{|\nabla H|} = \frac{-h_r \hat{\mathbf{r}} + \frac{1}{r} \hat{\boldsymbol{\theta}}}{\sqrt{h_r^2 + \frac{1}{r^2}}}, \quad \mathbf{t} = \frac{\frac{1}{r} \hat{\mathbf{r}} + h_r \hat{\boldsymbol{\theta}}}{\sqrt{h_r^2 + \frac{1}{r^2}}},$$

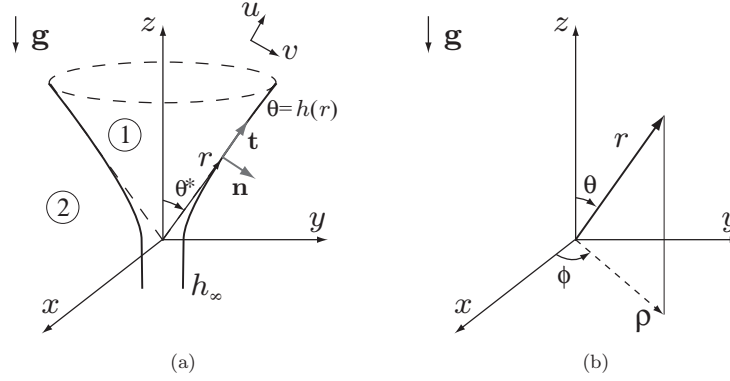


FIG. 2. Geometry of a steady tip-streaming: (a) cone set-up in spherical system of coordinates;  $\theta^*$  is the cone semi-angle, (b) spherical coordinates  $(r, \theta, \phi)$ ; the relation to the cylindrical system  $(\rho, \phi, z)$  is via  $x = \rho \cos \phi$ ,  $y = \rho \sin \phi$ , and  $z = z$ .

respectively, where  $\hat{\mathbf{r}}$  and  $\hat{\boldsymbol{\theta}}$  are unit vectors in the spherical coordinate system. The interfacial curvature is calculated via

$$\begin{aligned} \nabla \cdot \mathbf{n} &= \left[ \frac{1}{r^2} \frac{\partial}{\partial r} (r^2 n_r) + \frac{1}{r \sin \theta} \frac{\partial (\sin \theta n_\theta)}{\partial \theta} \right]_{\theta=h(r)} \\ &= \frac{\cot h - r \{h_r (3 + r h_r [2r h_r - \cot h]) + r h_{rr}\}}{r (1 + r^2 h_r^2)^{3/2}}, \end{aligned}$$

where  $n_r$  and  $n_\theta$  are  $r$ - and  $\theta$ -components of the normal vector  $\mathbf{n}$ , respectively; note that  $\mathbf{n}$  is directed from phase 1 to phase 2.

Since the tangential boundary condition (Marangoni stresses) drives the phenomena,<sup>10</sup> the appropriate non-dimensional notations (without introduction of new variables) read

$$r \rightarrow l_c r, \quad \mathbf{v} \rightarrow \frac{\sigma_{\max}}{\mu} \mathbf{v}, \quad p \rightarrow \frac{\sigma_{\max}}{l_c} p, \quad \sigma \rightarrow \sigma_{\max} \sigma, \quad \gamma \rightarrow \gamma_\infty \gamma, \quad (2)$$

where  $l_c = \sqrt{\sigma_{\max}/\rho g}$  is the capillary length,  $\mu$  the dynamic viscosity of each medium,  $\sigma_{\max}$  the interfacial tension in the clean interface case, and  $\gamma_\infty$  the saturation interfacial concentration. This choice of the characteristic length scale  $l_c$  is dictated by the following considerations. First, in the formulation there are no independent characteristic lengths as the drop is considered to be semi-infinite. However, in reality, the drop size is dictated by the balance of gravity and surface tension forces, which justifies the choice of the capillary length  $l_c$  as a characteristic length scale. The resulting value of the thread radius to be established in Sec. IV, where  $l_c$  is present, agrees with the observations on the order of magnitude, which *a posteriori* suggests that the chosen scaling is correct. Should the gravity play no role in our problem, tip-streaming would occur in any direction independent of the gravity vector, which was not witnessed in experiments.<sup>9</sup> However, there could be other regimes, where gravity is not responsible for the characteristic scale—after all, Marangoni-driven singularities may occur in a low-gravity environment—which can be due to, for example, the length scale set by the interplay of surfactant advection and kinetics and/or diffusion. These cases are not considered here.

### A. Velocity formulation

Let the  $(r, \theta)$ -velocity components be  $(u, v)$ , respectively. The continuity and momentum equations for each phase (omitting indexes) are given by

$$0 = \frac{1}{r^2} \frac{\partial (r^2 u)}{\partial r} + \frac{1}{r \sin \theta} \frac{\partial (\sin \theta v)}{\partial \theta}, \quad (3a)$$

$$\frac{L_r u}{\sqrt{Mo}} = -\frac{\partial p}{\partial r} + g_r + \Delta u - \frac{2u}{r^2} - \frac{2}{r^2 \sin^2 \theta} \frac{\partial(\sin \theta v)}{\partial \theta}, \quad (3b)$$

$$\frac{L_\theta v}{\sqrt{Mo}} = -\frac{1}{r} \frac{\partial p}{\partial \theta} + g_\theta + \Delta v + \frac{2}{r^2} \frac{\partial u}{\partial \theta} - \frac{v}{r^2 \sin^2 \theta}, \quad (3c)$$

where  $L_r u = (\mathbf{v}\nabla)u - v^2/r$  and  $L_\theta v = (\mathbf{v}\nabla)v + uv/r$  are the advection operators,  $g_r = -\cos \theta$  and  $g_\theta = \sin \theta$  the gravity vector projections,  $Mo = g\mu^4/(\rho\sigma^3)$  the Morton number, and the Laplacian  $\Delta$  is given by

$$\Delta = \frac{1}{r^2} \frac{\partial}{\partial r} \left( r^2 \frac{\partial}{\partial r} \right) + \frac{1}{r^2 \sin \theta} \frac{\partial}{\partial \theta} \left( \sin \theta \frac{\partial}{\partial \theta} \right).$$

The dynamic normal,  $[\mathbf{n} \cdot \mathbf{T} \cdot \mathbf{n}]_1^2 = \sigma \nabla \cdot \mathbf{n}$ , and tangent,  $[\mathbf{t} \cdot \mathbf{T} \cdot \mathbf{n}]_1^2 = -\mathbf{t}\nabla_s \sigma$ , interfacial boundary conditions at  $\theta = h(r)$  with the operator  $[f]_1^2 = f_2 - f_1$  and surface gradient  $\nabla_s = \mathbf{t} \cdot \nabla$ , can be written explicitly, taking into account that the stress tensor components are

$$T_{rr} = -p + 2\frac{\partial u}{\partial r}, \quad T_{r\theta} = \left( \frac{1}{r} \frac{\partial u}{\partial \theta} + \frac{\partial v}{\partial r} - \frac{v}{r} \right), \quad T_{\theta\theta} = -p + 2\left( \frac{u}{r} + \frac{1}{r} \frac{\partial v}{\partial \theta} \right).$$

As a result, the dimensionless dynamic normal and tangent conditions become

$$[p]_1^2 = -\sigma \nabla \cdot \mathbf{n} + \frac{2}{h_r^2 + \frac{1}{r^2}} \left[ h_r^2 \frac{\partial u}{\partial r} - \frac{h_r}{r} \left( \frac{1}{r} \frac{\partial u}{\partial \theta} + \frac{\partial v}{\partial r} - \frac{v}{r} \right) + \frac{1}{r^2} \left( \frac{u}{r} + \frac{1}{r} \frac{\partial v}{\partial \theta} \right) \right]_1^2, \quad (4a)$$

$$-\frac{\partial \sigma}{\partial r} = \frac{r}{\sqrt{h_r^2 + \frac{1}{r^2}}} \left[ -2\frac{h_r}{r} \left( \frac{\partial u}{\partial r} - \frac{u}{r} - \frac{1}{r} \frac{\partial v}{\partial \theta} \right) + \left( \frac{1}{r} \frac{\partial u}{\partial \theta} + \frac{\partial v}{\partial r} - \frac{v}{r} \right) \left( \frac{1}{r^2} - h_r^2 \right) \right]_1^2, \quad (4b)$$

respectively. As it will be useful for the subsequent discussion in Sec. III, it is worth commenting on the sign in the tangential dynamic boundary condition (4b), which can be done with the help of a local analysis in Figure 3. Namely, if we consider the interface as locally flat,  $h_r = 0$ , and phase 1 inertialess, then the tangential boundary condition (4b) becomes

$$n_\theta T_{r\theta t_r} = -\frac{\partial \sigma}{\partial r} \Rightarrow \left[ \frac{1}{r} \frac{\partial u}{\partial \theta} + \frac{\partial v}{\partial r} - \frac{v}{r} \right]_1^2 = -\frac{\partial \sigma}{\partial r}. \quad (5)$$

If the surfactant is “standard,” i.e., it lowers the surface tension, then from Figure 3 it follows that  $\partial \sigma / \partial r$  must be  $>0$  in order to drive  $\partial u / \partial \theta < 0$ , which conforms to the tangential boundary condition (4b) used below. The sign of  $\sigma$  in the tangential boundary condition (4b) should be changed in the case of an “inverse” surfactant, i.e., which increases the surface tension.<sup>28</sup>

The condition of the continuity of velocity across the interface is of the form

$$\mathbf{u} = (u, v) \equiv (u, v)_1 = \left( \frac{Mo_1}{Mo_2} \right)^{1/4} (u, v)_2. \quad (6)$$

The kinematic boundary condition,  $\mathbf{u} \cdot \mathbf{n} = 0$ ,

$$u \frac{\partial h}{\partial r} = \frac{1}{r} v, \quad (7)$$

where the velocity field corresponds to phase 1, completes the standard interfacial boundary conditions formulation.

Finally, while in the construction of self-similar solutions (Secs. III A and III B), we treat the singularity phenomena as generic here, i.e., independent of a particular interfacial material behavior, in order to understand the limits of applicability of such solutions and to match them to the thread solutions we will need to close the problem by adding the material behavior  $\sigma(\gamma)$  and

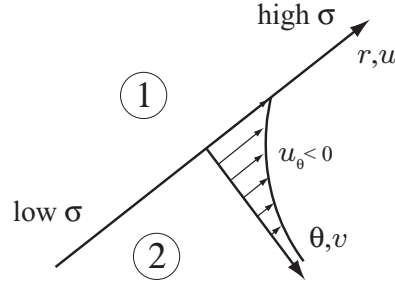
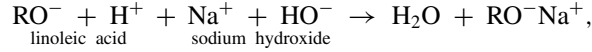


FIG. 3. On the sign in the tangential boundary condition (4b).

(non-dimensionalized) transport equation for the surfactant concentration  $\gamma$ ,

$$\nabla_s \cdot (\gamma \mathbf{u}_s) = \frac{1}{Pe_s} \nabla_s^2 \gamma + j_s, \quad (8)$$

where  $j_s$  is the flux due to chemical reaction,  $\mathbf{u}_s$  the interfacial velocity, and  $Pe_s$  the interfacial Peclet number. We assume that the surfactant is insoluble, as in the experiments of Fernandez and Homsy.<sup>9</sup> The details on the chemistry of the reaction at the oil-water interface between linoleic (fatty) acid and sodium hydroxide can be found in Chiwetelu *et al.*<sup>34</sup> Simplified, the reaction is



where it is assumed that recombination of  $\text{H}^+$  and  $\text{HO}^-$  and that of  $\text{Na}^+$  and  $\text{RO}^-$  dominate any others. In particular, the last interfacial reaction produces a tight, undissociated sodium salt, so that the insoluble surfactant becomes surface inactive. This salt partially remains at the interface and partially diffuses into the oil phase. In this paper, however, we are not concerned with the details of the surfactant production, but rather focus on the generic Marangoni-driven singularity formation phenomena. The effect of surfactant transport and realistic material behavior on interpretation of the self-similar solutions constructed in Sec. III will be discussed in Sec. III C.

## B. Governing parameters

In what follows, it will be assumed that the ratio of dimensional minimum and maximum values of interfacial tension is  $\sigma_{\min}/\sigma_{\max} \ll 1$ ; from now on we will designate  $\sigma_{\min}$  and  $\sigma_{\max} \equiv 1$  as non-dimensional quantities. We will also assume

$$Mo_1 \gg 1, \quad Mo_2 \gg 1,$$

which corresponds to the Stokes approximation in both phases, since the inertia in momentum equations is neglected. While, as mentioned in Introduction, it is known that the externally driven tip-streaming occurs only if the ratio of viscosities  $\mu_1/\mu_2$  (and thus  $Mo_1/Mo_2$ ) is small enough (actually  $< 0.1$  after the work of Taylor<sup>12</sup>),

$$\frac{\mu_1}{\mu_2} = \left( \frac{Mo_1}{Mo_2} \right)^{1/4} \equiv \delta \ll 1, \quad (9)$$

the analysis below will show that this restriction is not necessary for the Marangoni-driven tip-streaming.

## C. Stream-function formulation

Introducing a stream-function  $\Psi$  as

$$v_r \equiv u = \frac{1}{r^2 \sin \theta} \frac{\partial \Psi}{\partial \theta}, \quad v_\theta \equiv v = -\frac{1}{r \sin \theta} \frac{\partial \Psi}{\partial r}, \quad (10)$$

the creeping flow limit allows one to reduce problem (II A) to the biharmonic equation for  $\Psi$  in each phase,

$$E^2\Psi = 0, \text{ where } E = \frac{\partial^2}{\partial r^2} + \frac{\sin\theta}{r^2} \frac{\partial}{\partial\theta} \left( \frac{1}{\sin\theta} \frac{\partial}{\partial\theta} \right). \quad (11)$$

Given the velocity field one can determine the pressure field using

$$\frac{\partial p}{\partial r} = g_r + \frac{1}{r^2 \sin\theta} \frac{\partial}{\partial\theta} E\Psi, \quad (12a)$$

$$\frac{1}{r} \frac{\partial p}{\partial\theta} = g_\theta - \frac{1}{r \sin\theta} \frac{\partial}{\partial r} E\Psi, \quad (12b)$$

which are the compatibility conditions between the pressure and velocity fields to be used later. Note that  $dp = p_\theta d\theta + p_r dr$  is exact if there exists  $\Psi$  which solves (11). One can scale out the hydrostatic component of the pressure from (12) by the transformation

$$p_i = -r \cos\theta + \tilde{p}_i. \quad (13)$$

Another way to find the pressure is to solve the Laplace equation for  $\tilde{p}$  (note that the Laplacian is different from the operator  $E$  defined above)

$$\frac{1}{r^2} \frac{\partial}{\partial r} \left( r^2 \frac{\partial \tilde{p}}{\partial r} \right) + \frac{1}{r^2 \sin\theta} \frac{\partial}{\partial\theta} \left( \sin\theta \frac{\partial \tilde{p}}{\partial\theta} \right) = 0. \quad (14)$$

### III. SELF-SIMILAR SOLUTIONS

A general solution of (11) in spherical coordinates, cf. Figure 2(b), is<sup>35</sup>

$$\begin{aligned} \Psi = & \sum_{n=0}^{\infty} (A_n r^n + B_n r^{-n+1} + C_n r^{n+2} + D_n r^{-n+3}) \Phi_n(x) \\ & + \sum_{n=2}^{\infty} (A'_n r^n + B'_n r^{-n+1} + C'_n r^{n+2} + D'_n r^{-n+3}) \mathcal{H}_n(x), \end{aligned}$$

where  $x = \cos\theta$ ,  $\Phi_n(x)$ , and  $\mathcal{H}_n(x)$  are the Gegenbauer functions of the first and second kind, respectively. Based on this fact one can expect that self-similar solutions should be of the form

$$\Psi(r, \theta) = r^n \varphi(\cos\theta), \quad n \in \mathbb{Z}, \quad (15)$$

which are singular at  $r = 0$  for  $n \leq 1$  and thus observable only away from the tip singularity; the interface shape is then given by  $h(r) = \theta^* = \text{const.}$

Since we are interested in the leading order behavior, it makes sense to focus on the lowest positive powers of  $r$  similar to the analysis of Landau and Lifshitz<sup>36</sup> for the potential flow around a corner. This is justified by the following considerations. Let us first discuss the powers  $n \geq 1$ , the first three of which give:

- (1)  $\Psi(r, \theta) = r\varphi(\cos\theta)$ ,  $\tilde{p} = \pi(\cos\theta)/r^2$ , and thus  $\sigma \sim r^{-1}$ , the physics of which makes sense since the interfacial tension drives the Marangoni flow towards the tip, as observed experimentally, but the velocity field of the self-similar solution is singular at  $r = 0$ . Note that the velocity field of the self-similar solution of these conical vortices<sup>37</sup> diverges as  $r \rightarrow 0$ , which is the usual behavior of self-similarities, e.g., the Jeffrey–Hamel flow in converging channels or the flow around the corner (of angle  $< \pi$ ) as discussed by Landau and Lifshitz.<sup>36</sup>
- (2)  $\Psi(r, \theta) = r^2\varphi(\cos\theta)$ ,  $\tilde{p} = \pi(\cos\theta)/r$ , and thus  $\sigma = \text{const.}$ , which is the lowest power such that the velocity field may be expected to be non-singular at  $r = 0$ , but the pressure is still unbounded.

- (3)  $\Psi(r, \theta) = r^3 \varphi(\cos \theta)$ ,  $\tilde{p} = \pi(\cos \theta)$  or  $\tilde{p} = \pi(\cos \theta) \cdot \ln r$  and thus  $\sigma \sim r$ , the physics of which may make sense near the tip since the highly curved tip requires ultra-low interfacial tension to support it, but the Marangoni-induced flow is in the direction opposite to the observed one.

As indicated above, the case  $n = 1$  conforms with the experimental observation that the flow is driven from the base of the drop towards its tip. While the case  $n = 2$  gives the same general solution of (11) for the stream-function  $\Psi$  as for  $n = 1$ , the pressure ends up being constant due to the compatibility conditions (12). As a result, the solution develops a singularity along the axis of symmetry,  $\theta = 0$ , which cannot be compensated by a nonuniform pressure distribution as in the case  $n = 1$ . The along-the-axis singularity is observed for higher positive  $n$ 's as well, i.e.,  $n > 1$  gives non-physical solutions singular at  $\theta = 0$  and this singularity is non-removable. Thus, among positive  $n$ 's,  $n = 1$  is the only possible solution. Also, the case  $n = 1$  is the lowest order solution in the following senses: (a)  $\sigma \sim r^{-1}$  is the slowest decay of interfacial tension as  $r \rightarrow \infty$ , which allows for the flow towards the drop tip; (b)  $\psi \sim r$  is the least singular at  $r = 0$ .

While the “harmonics” corresponding to  $n < 1$  give velocity and pressure fields, which are also non-singular at the axis of symmetry, and contribute to the interfacial tension at a higher order  $\sigma \sim r^{-n}$ , we construct only the leading order solution here. Therefore, the focus of the subsequent discussion is on the case  $n = 1$ . The use of other “harmonics”  $n < 1$  will be commented on in Sec. III C.

### A. Two-phase solution, $n = 1$

The experimental observations of the conical drop shape, cf. Figure 1(a), suggest that the solution behaves in a self-similar fashion (ideal cone in Figure 2(a)), except for the regions near the tip and the base of the drop, so the goal here is to construct this self-similar solution and to identify the limits of its applicability. Under the condition  $n = 1$  following the work of Krechetnikov and Homsy,<sup>10</sup> the solution in a self-similar region is given by (dropping indices corresponding to each phase)

$$\Psi = r\varphi(x), \quad \tilde{p} = \frac{1}{r^2}\pi(x), \quad \sigma = \frac{\tilde{\sigma}_{\min}}{r}, \quad (16)$$

with independent variable  $x = \cos \theta$  and the constant  $\tilde{\sigma}_{\min}$  to be determined in Sec. III D. The velocities defined by (10) are singular at  $r = 0$ . As suggested by the structure of the solution (16), it belongs to the class of convergent flows, e.g., the Jeffrey-Hamel and Taylor cones solutions, but the interfacial tension gradients effect differentiates our solution from these in a fundamental way. In agreement with intuition, the infinitely sharp conical tip at  $r \rightarrow 0$  is supported by infinite surface tension in (16); the other intuitive possibilities corresponding to  $n \geq 3$ , which would allow  $\sigma \rightarrow 0$  as  $r \rightarrow 0$ , are excluded here because of the along-the-axis singularity and the wrong direction of the Marangoni flow.

Substitution of (16) into biharmonic equation for each phase (11) produces a simple equation (omitting the phase indexes)

$$(1 - x^2)\varphi^{(4)} - 4x\varphi^{(3)} = 0, \quad (17)$$

and the normal and tangential dynamic boundary conditions at the cone interface  $x = \xi = \cos \theta^*$ ,

$$[\pi(\xi)]_1^2 - \frac{2\xi}{1 - \xi^2} [\varphi(\xi)]_1^2 = -\frac{\tilde{\sigma}_{\min} \xi}{\sqrt{1 - \xi^2}}, \quad (18a)$$

$$\tilde{\sigma}_{\min} = \frac{1}{\sqrt{1 - \xi^2}} [2\varphi + (1 - \xi^2)\varphi']_1^2, \quad (18b)$$

respectively, where we used the fact that the curvature of the cone is  $\nabla \cdot \mathbf{n} = \cot \theta^*/r$ . Integrating (17) three times, we get

$$(1 - x^2)\varphi' + 2x\varphi = -[C_0 + C_1x + C_2x^2],$$

the general solution of which in each phase

$$\begin{aligned}\varphi &= (1-x^2) \left[ C - \int \frac{C_0 + C_1x + C_2x^2}{(1-x^2)^2} dx \right] \\ &= \frac{1}{2} \{ -(C_0 - C_2)(1-x^2) \operatorname{Arcth} x + 2C(1-x^2) - [C_1 + (C_0 + C_2)x] \},\end{aligned}\quad (19)$$

where  $C, C_{0,1,2}$  are constants and

$$\operatorname{Arcth} x = \frac{1}{2} \log \frac{1+x}{1-x}, \quad |x| < 1.$$

The function  $\operatorname{Arcth} x$  clearly has singularities at the axis of symmetry, i.e., at  $\theta = 0, \pi$ , but, as we will see from the subsequent analysis, the resulting solution for  $\varphi_{1,2}(x)$  is non-singular (this applies only to the case  $n = 1$ , while for other positive  $n$ 's the singularities are not removable as mentioned earlier). After the introduction of self-similarity variables into Eq. (14), the pressure is governed by

$$(1-x^2)\pi'' - 2x\pi' + 2\pi = 0. \quad (20)$$

Integration of (20) produces for each phase

$$\pi(x) = D_1x + D_2[x \operatorname{Arcth} x - 1]. \quad (21)$$

The compatibility of pressure with the velocity field (12) yields

$$D_1 = 2C, \quad D_2 = C_2 - C_0. \quad (22)$$

The system is completed with the velocity continuity conditions at the cone interface  $x = \xi$ ,

$$\varphi'_1(x) = \delta\varphi'_2(x) = 0, \quad (23a)$$

$$\varphi_1(x) = \delta\varphi_2(x), \quad (23b)$$

and zero stream-function designations at the cone boundary

$$x = \xi : \varphi_1 = \varphi_2 = 0, \quad (24)$$

and the axes of symmetry

$$x = 1 : \varphi_1 = 0, \quad (25a)$$

$$x = -1 : \varphi_2 = 0, \quad (25b)$$

of the drop and outer phase, respectively. Let us now count the number of constants and conditions on them:

- The velocity field in each phase gives four constants  $C$  and  $C_{0,1,2}$  (eight altogether); the pressure constants  $D_{1,2}$  are expressed in terms of  $C$  and  $C_{0,2}$ . Thus, we have eight independent constants.
- The number of independent boundary conditions is seven: normal (18a) and tangential (18b) at the interface, three velocity continuity conditions (23) at the interface, and two zero stream-functions at the axis of symmetry (25).

Thus there are more constants than conditions. Because the general solutions for velocity and pressure fields have singularity at the axis of symmetry,  $\theta = 0, \pi$ , it is desirable to eliminate it. Since physically the singular behavior seems to be resolved in the inner phase, i.e., by formation of a thread, then it makes sense to eliminate the singularity in the drop phase, which imposes the condition of boundedness of the velocity field,  $\partial_x\varphi_1$ , at the axis of symmetry  $x = 1$  (drop), which in turn gives  $C_0 = C_2$ ; the pressure in the drop is non-singular then too. Therefore, the number of independent constants is now equal to the number of conditions.

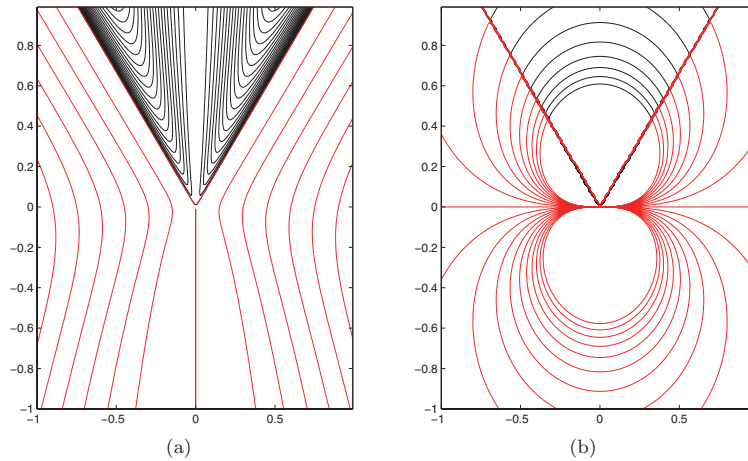


FIG. 4. (Color online) Two-phase self-similar solution: plots of (a) the streamlines, (b) the isobars.

Note that the condition (23b) coincides with (24), and the kinematic condition,  $\varphi_1 = 0$ , is just trivial and contained in (24). The use of all boundary conditions yields for the drop phase

$$\varphi_1 = \frac{\tilde{\sigma}_{\min} \delta (1-x)(x-\xi)}{2 \sqrt{1-\xi^2}} \frac{1+\xi}{1+\delta-\xi(1-\delta)}, \quad (26a)$$

$$\pi_1 = \tilde{\sigma}_{\min} \frac{\delta x \sqrt{1-\xi^2}}{(1-\xi)^2 + \delta(1-\xi^2)}, \quad (26b)$$

and for the outer phase

$$\varphi_2 = \frac{\tilde{\sigma}_{\min} (1+x)(x-\xi)}{2 \sqrt{1-\xi^2}} \frac{1-\xi}{1+\delta-\xi(1-\delta)}, \quad (27a)$$

$$\pi_1 = -\tilde{\sigma}_{\min} \frac{x \sqrt{1-\xi^2}}{\sqrt{1+\xi}(1-\xi+\delta(1+\xi))}, \quad (27b)$$

which are the velocity and pressure fields, respectively. Note that the velocity fields are bounded at infinity, as follows from (10), and non-singular at the axis of symmetry as opposed to the solutions found earlier in Krechetnikov and Homsy;<sup>10</sup> the latter discrepancy is due to the difference in sign in the tangential boundary conditions used in Krechetnikov and Homsy<sup>10</sup> and here, respectively. The resulting solution (26)–(27) is plotted in Figure 4 in polar coordinates  $(r, \theta)$  as

$$\Psi_i(r, \theta) = r \varphi_i(\cos \theta), \quad \tilde{p}_i = \frac{1}{r^2} \pi_i(\cos \theta).$$

As mentioned in Introduction, while the flow pattern in Figure 4(a) is analogous to that in Taylor cones,<sup>38,39</sup> the underlying physics is different as discussed in Sec. I C.

## B. One-phase solution

One-phase solutions satisfy the same boundary conditions—normal (18a) and tangential (18b) dynamic conditions, compatibility of the pressure and velocity fields (22), zero stream-function at the cone boundary (24) and the axes of symmetry (25)—with the exception of the velocity continuity conditions (23).

The resulting solution in the outer phase is given by

$$\varphi_2 = \frac{\tilde{\sigma}_{\min} (1+x)(x-\xi)}{2 \sqrt{1-\xi^2}}, \quad (28a)$$

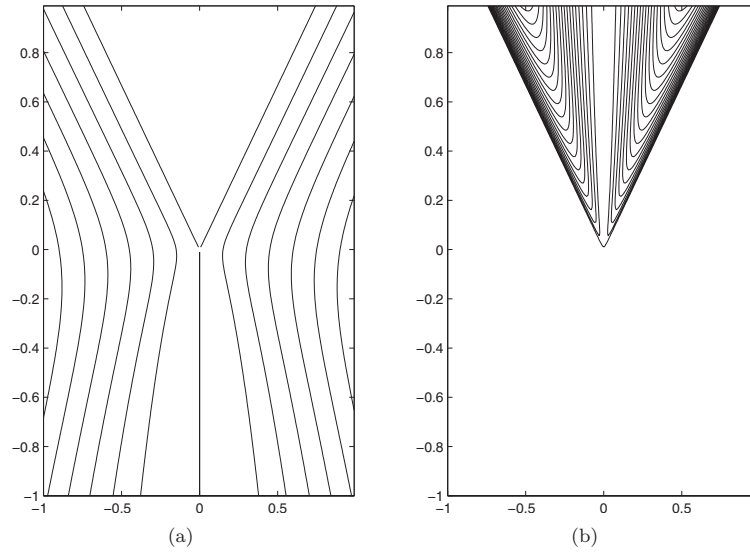


FIG. 5. Streamline fields for one-phase solutions: (a) outer phase, (b) inner phase.

$$\pi_2 = -\tilde{\sigma}_{\min} \frac{x}{\sqrt{1-\xi^2}}, \quad (28b)$$

which can also be obtained from (27) in the limit  $\delta \rightarrow \infty$ . The corresponding streamline pattern is illustrated in Figure 5(a). Similarly, one can construct the non-singular solution in the inner phase (when the outer phase is considered inviscid and inertialess),

$$\varphi_1 = \frac{\tilde{\sigma}_{\min}}{2} \frac{(1-x)(x-\xi)}{\sqrt{1-\xi^2}}, \quad (29a)$$

$$\pi_1 = \tilde{\sigma}_{\min} \frac{x}{\sqrt{1-\xi^2}}, \quad (29b)$$

which can also be obtained from (26) in the limit  $\delta \rightarrow 0$  and which is shown in Figure 5(b). One can also view the solutions (28)–(29) as a result of application of the Principle of equivalence of one- and two-phase Stokes flow motions (Proposition 1). As mentioned in Sec. I B, if the viscosity of an equivalent one-phase system is negative, then the interfacial tension should have an opposite sign. Here, without loss of generality, we will consider the case when the one-phase system, either resulting from reduction of a two-phase system by Proposition 1 or if the outer phase is absent in the original physical system, has a positive viscosity and thus the sign of interfacial tension is standard. The same assumption will be carried over to Sec. IV, where we construct the thread solution.

If one uses the sign in the tangential boundary condition (4b) corresponding to an “inverse” surfactant, then the singularity appears not only at the tip of the drop but also at the axis of symmetry;<sup>10</sup> for example, in the case when the phase in the drop is considered inertialess, then the outer solution is still singular at the axis of symmetry and given by

$$\varphi_2 = -\frac{\tilde{\sigma}_{\min}}{2} \frac{(1+x)(x-\xi)(1-2\xi^2)}{\sqrt{1-\xi^2}} + \tilde{\sigma}_{\min} \xi \sqrt{1-\xi^2} (1-x^2) (\text{Arcth } x - \text{Arcth } \xi), \quad (30)$$

$$\pi_2 = \tilde{\sigma}_{\min} \frac{x(1-2\xi^2) - 2\xi(1-\xi^2)}{\sqrt{1-\xi^2}} + 2\tilde{\sigma}_{\min} x \xi \sqrt{1-\xi^2} (\text{Arcth } x - \text{Arcth } \xi). \quad (31)$$

Since there are no experiments with inverse surfactants in the situations analogous to the considered here, the true nature of singularity in (30) is not clear, but one can offer the following potential explanations for the presence of this mathematical singularity:

- Flow is nonlinear (non-Stokes) at the axis of symmetry.
- Steady self-similar solution does not exist, i.e., the solution realizes only in an unsteady fashion.

### C. On the existence and implications of self-similar solutions

The constructed Marangoni-driven self-similar solutions (16) are generic, i.e., independent of a particular source of the interfacial tension variation (temperature, surfactant concentration, electric field, etc.). In general, it is known that self-similar behavior near (interfacial) singularities is consistent with the fact that interfacial tension plays the smoothing role due to its tendency to minimize the surface area and with the general theoretical understanding that if there are no physically relevant characteristic length scales in the problem (when the drop is considered to be semi-infinite), then the solution behaves self-similarly.<sup>40,41</sup>

As any other self-similar solutions, e.g., the Jeffrey-Hamel flow in a converging channel, the ones constructed above are an idealization in the sense that real fluid properties (including interfacial tension) cannot support the existence of the singularity. However, self-similar solutions are useful constructions which capture the flow “in large” and thus provide reasonable approximations to observable flows away from singularities. In our situation, the self-similar solution—the conical drop and the flow structure—is suggested by experimental observations.<sup>9</sup>

From the physical considerations and the form of the self-similar solution (16), in particular  $\sigma = \tilde{\sigma}_{\min}/r$ , it is evident *a priori* that this solution breaks down for  $r = \tilde{\sigma}_{\min}$  and  $\tilde{\sigma}_{\min}/\sigma_{\min}$  as the value of the interfacial tension cannot go above its maximum  $\sigma_{\max} \equiv 1$  and below minimum  $\sigma_{\min}$  values; then  $\tilde{\sigma}_{\min} \geq \sigma_{\min}$  in (16) has the meaning of the minimum interfacial tension achieved at the base of the drop, where self-similarity breaks down. This is consistent with the fact that the interfacial stretching is the weakest at the base of the drop, where it attached to a nozzle (cf. Figure 1(a)), so that the chemical reaction produces the maximum surfactant concentration in this region giving the minimum value  $\tilde{\sigma}_{\min}$  of the interfacial tension.

Therefore, the constructed self-similar solution (16) is valid in the intermediate asymptotics sense,<sup>41</sup> i.e., for  $\sigma_{\min} < r < \tilde{\sigma}_{\min}/\sigma_{\min}$  but not for all  $r$ 's. Given the equation of state  $\sigma(\gamma)$  and the self-similar form (16), the distribution of  $\gamma$  over this interval of  $r$ 's is given, in general, by the inverse function

$$\gamma(r) = \sigma^{-1} \left( \frac{\tilde{\sigma}_{\min}}{r} \right), \quad (32)$$

which is a *necessary* condition for the observation of a conical shape driven by Marangoni effects. Since  $\sigma(\gamma)$  is unknown for the chemical reaction used in experiments,<sup>9</sup> for concreteness of the discussion we will consider a power-law approximation of the material behavior

$$\sigma \sim \gamma^{-1/\zeta}, \quad (33)$$

on such an interval of  $r$ 's over which self-similar behavior is observable, cf. Figure 6 and further discussion in Sec. III D. It must be emphasized that as opposed to the above stated general necessary condition (32) for the existence of a conically symmetric solution, the form (33) is not necessary as there may exist other forms of  $\sigma(\gamma)$  producing  $\sigma \sim r^{-1}$  in (16). In fact, as follows from (32), there exist an infinite number of other forms of  $\sigma(\gamma)$  which produce self-similar behavior (16);  $\gamma(r)$  need not behave self-similarly, though. As for the concrete form (33), the exact power-law form of the equation of state  $\sigma(\gamma)$  is not crucial for the existence of a self-similar solution—as long as (a) the problem is well-posed in Hadamard's sense<sup>42</sup> and thus not very sensitive to a variation of the coefficients (e.g., material behavior) in the equations, and (b)  $\sigma(\gamma)$  is close to the power-law form for some range of  $\gamma$ 's—the solution will then stay close to the ideal self-similar form (16). As mentioned above, the found self-similar solution is alike the experimentally observed conical drops,

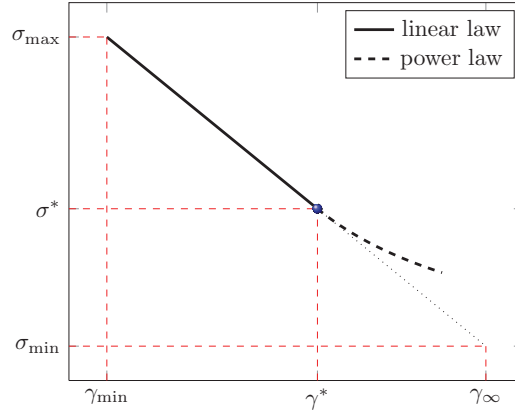


FIG. 6. (Color online) Composite (linear + power law) approximation of material behavior  $\sigma(\gamma)$ . The dot on the plot corresponds to the point  $\gamma^*$ , where linear and power laws match.

cf. Figure 1(a); this similarity will be further reinforced by a construction of the thread solution (cf. Sec. IV B), which matches to the conical shape of the drop.

Therefore, the question of existence of a self-similar solution to the problem involving surfactant transport (8) and realistic material behavior  $\sigma(\gamma)$  can be approached from two viewpoints. First of all, the work of Fernandez and Homsy<sup>9</sup> suggested the existence of a self-similar solution—the cone shape of the drop in the steady tip-streaming regime—empirically. Second, the following simple theoretical considerations support the existence of the surfactant distribution  $\gamma(r)$ , which allows the self-similarity to be observable for a range of  $r$ 's.

The interfacial surfactant transport Eq. (8) on a cone shaped surface,  $h_r = 0$ , in spherical coordinates and in the non-dimensional form can be written as

$$\frac{1}{r} \frac{\partial}{\partial r} (r\gamma u_s) = \frac{1}{Pe_s} \frac{1}{r} \frac{\partial}{\partial r} \left( r \frac{\partial \gamma}{\partial r} \right) + j_s, \quad (34)$$

where  $u_s = -\tilde{\sigma}_{\min}(1 - \xi)/(2r)$  is the interfacial velocity obtained from (29). Note that the surface divergence  $\nabla_s \cdot \mathbf{T}$  of the surface vector  $\mathbf{T} = \gamma \mathbf{u}_s$  in (8) is calculated according to tensor analysis<sup>43</sup> on a Riemannian manifold (in our case, it is a two-parameter surface embedded in three dimensional space defined by the position vector  $\mathbf{r}(u^1, u^2)$ , which is a function of free parameters  $u^1$  and  $u^2$ ). Namely,  $\nabla_s \cdot \mathbf{T}$  is the covariant derivative of a contravariant component of a vector field  $\mathbf{T} = T^i \mathbf{c}_i$  defined in the tangent space of the manifold,

$$\nabla_s \cdot \mathbf{T} = \partial_i T^i + \left\{ \begin{matrix} j \\ ij \end{matrix} \right\} T^j, \quad (35)$$

where  $\left\{ \begin{matrix} j \\ ij \end{matrix} \right\}$  is the Christoffel symbol of the second kind calculated generally via  $\left\{ \begin{matrix} k \\ ji \end{matrix} \right\} = \mathbf{c}^k \cdot \partial_j \mathbf{c}_i$ , where  $\partial_j = \partial/\partial u^j$  and the basis vectors  $\mathbf{c}_i = \partial_i \mathbf{r}(u^1, u^2)$  are the tangent vectors of the parameter curves in the surface. For our conical surface in spherical coordinates, cf. Figure 2(a), the surface is parameterized by  $u^1 = r$  and  $u^2 = \phi$  and the radius vector  $\mathbf{r}$  is given by (1).

The form of Eq. (34) suggests the power-law distribution of surfactant along the interface,

$$\gamma = d r^\zeta, \quad \zeta > 0, \quad \sigma_{\min} < r < \tilde{\sigma}_{\min}/\sigma_{\min}, \quad (36)$$

where the value of the exponent  $\zeta$  depends on the particularities of the equation of state  $\sigma(\gamma)$ . Thus, problem (34) has the particular solution (36) provided the interfacial flux has the form

$$j_s = b \gamma^{1-\frac{2}{\zeta}}, \quad (37)$$

such that the constant  $d$  in (36) is found by a direct balance of terms in (34). This power-law form of  $j_s$  can be justified from a more general expression for the surfactant flux (73) utilized in the thread

region analysis (Sec. IV B). If  $j_s = 0$ , then due to linearity of (34) in  $\gamma$ , the factor  $d$  is left arbitrary without extra conditions dictated by the physics of the problem (cf. Sec. IV B 3).

Above we constructed a concrete case which leads to self-similar behavior (16): as an example we used the equations of state (33), which together with the power-law solution (36) leads to  $\sigma \sim r^{-1}$  required for the self-similarity to exist. Consideration of a combination of a few higher order “harmonics”  $\sigma \sim r^{n-2}$  in conjunction with the corresponding self-similar solutions (15) may provide a better approximation of the material behavior  $\sigma(\gamma)$  and, based on the general properties of asymptotic series, should enlarge the range of  $r$ 's for which the self-similarity holds.

#### D. Equation of state

The considerations in Sec. III C of a particular form of the equation of state (33) in the self-similar (cone) region lead to the following discussion, which will be instrumental in the construction of the thread solution in Sec. IV and matching it to the cone solution.

First of all, it should be noted that in the case when surfactant is produced by a chemical reaction at the interface, interfacial tension is dynamic in general, i.e., it is a function of both surfactant concentration and time. In the steady case and when there is no interface stretching, one naturally gets  $\sigma = \sigma_{\min}$  everywhere at the interface since the chemical reaction continuously produces surfactant. In our case, the problem is steady, which justifies the use of steady versions of  $\sigma(\gamma)$  and  $j_s(\gamma)$ , but interface stretching results in a non-uniform tension distribution along the interface.

From a modeling prospective, there are no analytical expressions for equations of state valid over the entire range of surfactant concentrations—most common equations, e.g., the Frumkin-type state equation obtained from the Gibbs adsorption isotherm for an ideal solution,  $\sigma = \sigma_{\max} + 2\gamma_{\infty} RT \ln(1 - \gamma/\gamma_{\infty})$ <sup>44</sup> in dimensional variables, are valid only for dilute premicellar solutions,<sup>45</sup> here  $R$  is the gas constant,  $T$  is the temperature. This fact is obvious from the direct comparison with the experimental data for both ionic<sup>46</sup> and non-ionic surfactants<sup>47</sup> as well as from the diverging character of such equations as  $\gamma \rightarrow \gamma_{\infty}$ .<sup>48</sup> Equations such as Sheludko's one<sup>49,50</sup> often applied for non-dilute concentrations<sup>51</sup> are empirical and thermodynamically inconsistent with other models such as Langmuir isotherm required for surfactant transport modeling. Given experimental measurement points for  $\sigma(\gamma)$ , any function fit cannot give a unique state equation  $\sigma(\gamma)$  due to scatter of experimental data. In the case of the chemical reaction used in the work of Fernandez and Homsy,<sup>9</sup> there is no experimentally measured state equation as the surfactant is produced by the chemical reaction and is normally not present / used separately from the reaction itself; instead, there are only dynamic interfacial tension measurements,<sup>52,53</sup> which are not relevant to the present study. Therefore, a power-law form of  $\sigma(\gamma)$  cannot be excluded and likely exists for a certain range of  $\gamma$ 's (especially close to the saturation value  $\gamma_{\infty}$ ) as sketched in Figure 6, since the self-similar solution is observable experimentally.

As dictated by the experimental observations and the logical possibility that for some interval of  $\gamma$ 's the interfacial tension behaves in a self-similar fashion (33), one is lead to conclude that  $\sigma$  has a composite form shown in Figure 6. For simplicity and as a good approximation of the experimental data,<sup>46,47</sup> we will use the approximate linear equation of state,

$$\sigma = \sigma_{\max} + \gamma (\sigma_{\min} - \sigma_{\max}), \quad 0 \leq \gamma \leq \gamma^*, \quad (38)$$

and the power-law form (33). As pointed out in Sec. III C, this approximation is non-unique and without much effect on the solution,  $\sigma(\gamma)$  can be approximated by other functions as long as it stays close to the composite one. This composite form, of course, would come from the fit to data and thus implies that both  $\sigma$  and  $d\sigma/d\gamma$  should be continuous at the point of matching  $\gamma^*$ . The continuity of  $\sigma$  and  $\sigma_{\gamma}$  is required as both of them appear in the formulation of the problem, i.e., in the normal and tangential boundary conditions (4). Higher order continuity of the solution is achieved by constructing higher order corrections to  $\sigma(\gamma)$ .

Given the linear form (38) of  $\sigma$  and the power-law form (33),

$$\sigma(\gamma) = \frac{\tilde{\sigma}_{\min}}{(\gamma/d)^{1/\zeta}} \text{ with } \gamma = d r^\zeta, \quad (39)$$

we find from the continuity of  $\sigma$  at  $\gamma^*$  that

$$\tilde{\sigma}_{\min} = \sigma_{\max} \left( \frac{\gamma^*}{d} \right)^{1/\zeta} \frac{\zeta}{1 + \zeta}, \quad (40)$$

and from the continuity of  $d\sigma/d\gamma$  at  $\gamma^*$ ,

$$\gamma^* = \frac{1}{1 - \frac{\sigma_{\min}}{\sigma_{\max}}} \frac{1}{1 + \zeta}. \quad (41)$$

As a result, the equation of state for  $\gamma > \gamma^*$ , i.e., in the “power-law” region, is given by

$$\sigma(\gamma) = \sigma_{\max} \left( \frac{\gamma^*}{\gamma} \right)^{1/\zeta} \frac{\zeta}{1 + \zeta}, \quad \gamma^* \leq \gamma. \quad (42)$$

Note that, as it should be, the material behavior does not depend on the factor  $d$  as the latter is determined by the coupled hydrodynamics and surfactant transport.

It is remarkable that the derivative  $d\sigma/d\gamma$  is non-zero at  $\gamma = 0$  as opposed to the intuitive expectation, which can be explained from the standard models for soluble surfactants valid for dilute concentrations. Namely, when expressed in terms of the bulk concentration  $c$ , which is more suitable for the analysis of the interfacial material behavior, one gets

$$\frac{d\sigma}{d\gamma} = \frac{d\sigma}{dc} \frac{dc}{d\gamma} \text{ with } \frac{d\sigma}{dc} < 0 \text{ and } \frac{d\gamma}{dc} > 0. \quad (43)$$

Indeed, from the Szyszkowsky equation,  $\sigma = \sigma_{\max} - 2RT\gamma_{\infty} \ln(1 + K_L c)$  in dimensional variables, and the Langmuir isotherm,  $k_a c(1 - \gamma/\gamma_{\infty}) - k_d \gamma = 0$ , where  $K_L = k_a/(k_d \gamma_{\infty})$  is the Langmuir constant,  $k_a$  and  $k_d$  the adsorption and desorption coefficients, respectively, it follows that

$$\frac{d\sigma}{dc} = -2RT\gamma_{\infty} K_L \left( 1 - \frac{\gamma}{\gamma_{\infty}} \right) < 0. \quad (44)$$

Also,

$$\frac{dc}{d\gamma} = \frac{k_d}{k_a} \left( 1 - \frac{\gamma}{\gamma_{\infty}} \right)^{-2} > 0, \quad (45)$$

which together with (44) produces

$$\frac{d\sigma}{d\gamma} = -2RT \left( 1 - \frac{\gamma}{\gamma_{\infty}} \right)^{-1} < 0. \quad (46)$$

When evaluated at  $\gamma = 0$ , the derivative  $d\sigma/d\gamma$  is certainly non-zero.

Finally, note that as opposed to the above thermodynamic considerations of the derivative  $d\sigma/d\gamma$  at  $\gamma = 0$ , there are no known restrictions on  $\sigma(\gamma)$  to be convex  $\sigma_{\gamma\gamma} > 0$  or concave  $\sigma_{\gamma\gamma} < 0$  for the entire range of  $\gamma$ 's. Therefore, one cannot rule out the possible behavior shown in Figure 6.

## IV. THREAD SOLUTIONS

### A. General remarks

Due to the equivalence of one- and two-phase solutions (Proposition 1), we will construct a thread solution for one-phase system, when only the drop is in the Stokes regime, while the outer flow is inertialess and inviscid. The standard way to resolve the cone-tip singularity would be through the introduction of a transition region (II) similar to that in the Landau-Levich problem,<sup>25</sup> as shown on Figure 7, which matches the solution in the cone region (I), where the solution is self-similar, to that in the thread region (III), where the jet is of constant radius  $h_{\infty}$  as  $z \rightarrow -\infty$ .

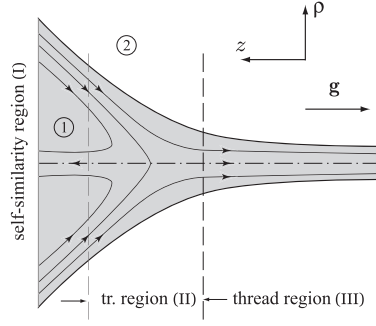


FIG. 7. On resolution of the singularity.

The presence of the stagnation point, cf. Figure 7, may appear to prevent one from application of the lubrication (slender jet) approximation since the assumption of a unidirectional flow built into the lubrication approximation is no longer valid. However, the recent work<sup>26</sup> demonstrates the applicability of lubrication approximations in such cases due to the weak ellipticity property of the lubrication equations. Moreover, explicit construction of the solution below will show that the lubrication approximation indeed captures the internal stagnation point.

In the construction of the thread solution, we can no longer use the idealized interfacial tension behavior,  $\sigma \sim r^{-1}$ , but rather should appeal to the true physical property of its boundedness from above and non-zero value at the minimum, cf. Figure 6. This is also necessary for correct prediction of the thread radius. These considerations, however, do not invalidate the constructed self-similar solution as the latter is valid in the intermediate asymptotics sense only (Sec. III C). Since interfacial tension is always bounded, in particular  $0 < \tilde{\sigma}_{\min} < 1$ , the self-similar solution (16) in Sec. III breaks when  $z \sim O(\tilde{\sigma}_{\min} \cos \theta^*)$ . Thus, one can distinguish three distinct regions:

- (I) Cone region:  $\rho, z \sim O(1)$ ;
- (II) Transition region:  $z \sim O(\tilde{\sigma}_{\min} \cos \theta^*)$ ,  $\rho \sim O(h_\infty)$ ; and
- (III) Slender jet region:  $\rho \ll z$ ,  $\rho \sim O(h_\infty)$ .

All these scalings, in particular  $z \sim O(\sigma_{\min})$ , will naturally follow from the asymptotic analysis. The scale  $h_\infty$  can be found only after matching the solution with the one in the cone region in analogy with the dip coating problem of Landau and Levich.<sup>25</sup>

## B. Asymptotic analysis

### 1. Scaling and problem statement

In view of the cylindrical symmetry of the thread solution, it is convenient to study it in the cylindrical system of coordinates:

$$x = \rho \cos \phi, \quad y = \rho \sin \phi, \quad z = z;$$

the geometry of the problem is sketched in Figure 8. The normal  $\mathbf{n}$  and tangent  $\mathbf{t}$  vectors to the interface,  $H = \rho - h(z) = 0$ , are given by

$$\mathbf{n} = \frac{\nabla H}{|\nabla H|} = \frac{\hat{\boldsymbol{\rho}} - h_z \hat{\mathbf{z}}}{\sqrt{1 + h_z^2}}, \quad \mathbf{t} = \frac{h_z \hat{\boldsymbol{\rho}} + \hat{\mathbf{z}}}{\sqrt{1 + h_z^2}}, \quad (47)$$

where  $\hat{\boldsymbol{\rho}}$  and  $\hat{\mathbf{z}}$  are unit vectors in the cylindrical coordinate system; note that the tangent vector  $\mathbf{t}$  has the same direction as in the spherical coordinates. The interfacial curvature is calculated via

$$\nabla \cdot \mathbf{n}|_{\rho=h(z)} = \left[ \frac{1}{\rho} \frac{\partial}{\partial \rho} (\rho n_\rho) + \frac{\partial n_z}{\partial z} \right]_{\rho=h(z)} = -\frac{h_{zz}}{(1 + h_z^2)^{3/2}} + \frac{1}{h\sqrt{1 + h_z^2}},$$

where  $n_\rho$  and  $n_z$  are  $\rho$ - and  $z$ -components of the normal vector  $\mathbf{n}$ , respectively.

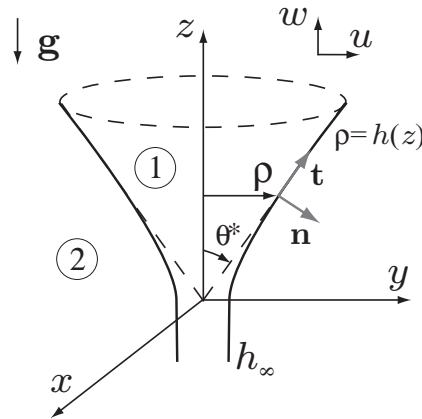


FIG. 8. Geometry of the problem in cylindrical coordinates.

The idea now is to analyze the solution in the neighborhood of the axis of symmetry with the goal of resolving the singularity via a construction of a jet solution. Let the velocity components be  $(u, w)$  along  $(\rho, z)$ -axes, respectively. Applying the following thin layer (or slender-jet) non-dimensionalization:

$$z \rightarrow l_c z, \quad \rho \rightarrow h_\infty \rho, \quad w \rightarrow \frac{\sigma_{\max}}{\mu} w, \quad u \rightarrow \epsilon \frac{\sigma_{\max}}{\mu} u, \quad p \rightarrow \kappa \frac{\sigma_{\max}}{l_c} p, \quad \sigma \rightarrow \sigma_{\max} \sigma, \quad \gamma \rightarrow \gamma_\infty \gamma, \quad (48)$$

where  $\epsilon = h_\infty / l_c \ll 1$  with  $h_\infty$  to be determined from scaling arguments, to the axisymmetric Navier–Stokes equations in cylindrical coordinates  $(\rho, z)$ , we obtain

$$0 = \frac{1}{\rho} \frac{\partial}{\partial \rho} (\rho u) + \frac{\partial w}{\partial z}, \quad (49a)$$

$$0 = -\frac{\partial p}{\partial \rho}, \quad (49b)$$

$$0 = -\frac{\partial p}{\partial z} + \frac{1}{\rho} \frac{\partial}{\partial \rho} \left( \rho \frac{\partial w}{\partial \rho} \right), \quad (49c)$$

which is just a set of standard lubrication equations; here we used the condition  $\kappa = \epsilon^{-2}$ , which follows from the slender jet assumption. The appropriate boundary conditions for (49) as  $z \rightarrow -\infty$  are (a)  $w \rightarrow w_\infty$  to be determined from matching and (b)  $p \rightarrow \text{const}$ . Note that the large scaling factor for the pressure  $\kappa = \epsilon^{-2}$  as opposed to the  $O(1)$ -factor in the cone region, cf. (2), can be explained by the fact that the flow in the cone region is driven by a smaller pressure gradient because of the geometry confining effect, while in the jet region one requires much larger pressure gradients to drive the flow. Introducing the stream-function  $\Psi$  in cylindrical coordinates,

$$u = \frac{1}{\rho} \frac{\partial \Psi}{\partial z}, \quad w = -\frac{1}{\rho} \frac{\partial \Psi}{\partial \rho}, \quad (50)$$

we get the general solution of (49),

$$\Psi(\rho, z) = -\frac{\rho^4}{16} \frac{\partial p}{\partial z} + C_0 + C_1 \rho^2 \log \rho + C_2 \rho^2, \quad (51)$$

where the constants are functions of  $z$ ,  $C_i = C_i(z)$ . The  $z$ -dependence of  $C_i$  turns out to be important for the construction of the solution in the thread region capable of capturing the flow topology shown in Figure 7.

The dynamic normal,  $\mathbf{n} \cdot \mathbf{T} \cdot \mathbf{n} = -\sigma \nabla \cdot \mathbf{n}$ , and tangential,  $\mathbf{t} \cdot \mathbf{T} \cdot \mathbf{n} = \mathbf{t} \nabla_s \sigma$ , boundary conditions at the interface  $\rho = h(z)$ , can be written explicitly, taking into account that the stress tensor components are

$$T_{\rho\rho} = -p + 2\frac{\partial u}{\partial \rho}, \quad T_{\rho z} = \frac{\partial w}{\partial \rho} + \frac{\partial u}{\partial z}, \quad T_{zz} = -p + 2\frac{\partial w}{\partial z},$$

so that in the dimensionless form, we get the normal

$$p + \sigma \left[ \epsilon^3 \frac{h_{zz}}{(1 + \epsilon^2 h_z^2)^{3/2}} - \frac{\epsilon}{h \sqrt{1 + \epsilon^2 h_z^2}} \right] = \frac{2\epsilon^2}{1 + \epsilon^2 h_z^2} [u_\rho - h_z(\epsilon^2 u_z + w_\rho) + \epsilon^2 h_z^2 w_z],$$

and tangential

$$\sqrt{1 + \epsilon^2 h_z^2} \sigma_z = [2\epsilon h_z (u_\rho - w_z) + (1 - \epsilon^2 h_z^2)(\epsilon u_z + \epsilon^{-1} w_\rho)],$$

dynamic conditions, respectively. The kinematic boundary condition

$$u - wh_z = 0, \quad (52)$$

completes the standard interfacial boundary conditions formulation.

## 2. Slender-jet approximation

The leading order asymptotic forms of the normal, tangential, and kinematic conditions relevant to our subsequent analysis are

$$-p + \sigma \left[ \frac{\epsilon}{h \sqrt{1 + \epsilon^2 h_z^2}} - \epsilon^3 h_{zz} \right] = -2\epsilon^2 [u_\rho - h_z w_\rho] + O(\epsilon^4), \quad (53a)$$

$$w_\rho = \epsilon \sigma_z + O(\epsilon^2), \quad (53b)$$

$$u - wh_z = 0, \quad (53c)$$

respectively. Note the sign in the tangential dynamic condition (53b), which is explained in Figure 9: both  $\sigma_z$  and  $w_\rho$  are negative. It is also remarkable that the second curvature (the first term in the square brackets on the left hand-side) dominates the asymptotics, which is common for slender-jet axisymmetric problems. In addition, there are conditions of no singularity, which give  $C_1 = 0$  in (51), and the symmetry conditions,

$$r = 0 : u = 0, \quad w_\rho = 0, \quad (54)$$

from which it follows that  $C_0 = \text{const.}$  in (51). Next, the condition of a constant stream-function along the interface  $\rho = h(z)$  furnishes  $\Psi(\rho, z)|_{\rho=h(z)} = \Psi(\rho, -\infty)|_{\rho=\hat{h}_\infty}$  and thus from (51), we obtain

$$-\frac{h^4}{16} \frac{\partial p}{\partial z} = C_2^\infty \hat{h}_\infty^2 - C_2(z) h^2, \quad (55)$$

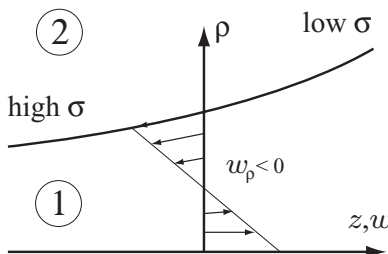


FIG. 9. On the sign in the tangential boundary condition (53b).

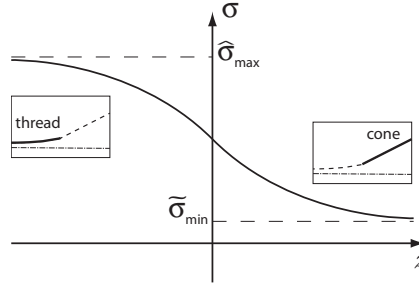


FIG. 10. Variation of the interfacial tension along the interface.

where  $C_2^\infty = C_2(-\infty)$  and  $\widehat{h}_\infty = h(-\infty)$  is an  $O(1)$ -parameter, which can be set to one by a proper choice of scaling as will be shown below. From now on, to avoid confusion, we will be denoting the key variables in the limit  $z \rightarrow -\infty$  with hats, in particular  $\widehat{\sigma}_{\max} = \sigma(\widehat{\gamma}_{\min})$ . The value of the constant  $C_2^\infty$  is determined from the flux in the thread at  $z = -\infty$ , where the fluid velocity is uniform across the thread and equals to  $w_\infty < 0$ ,

$$0 > \lim_{z \rightarrow -\infty} \int_0^h w \cdot 2\pi\rho \, d\rho = -2\pi \Psi|_0^{\widehat{h}_\infty} = -2\pi C_2^\infty \widehat{h}_\infty^2 = w_\infty \cdot \pi \widehat{h}_\infty^2, \quad (56)$$

i.e.,  $C_2^\infty = -w_\infty/2$ .

Next, from compatibility of the leading normal (53a),  $p = \epsilon \sigma/h$ , and tangential (53b),  $w_\rho = \epsilon \sigma_z$ , interfacial boundary conditions it follows that the interfacial shape is given by

$$h(z) = \frac{c}{\sigma(z)}, \quad (57)$$

where  $c$  is a constant to be determined. Thus, the solution, which connects both the cone and thread regions exists due to the capillary and Marangoni forces, which in turn arise due to the varying  $\sigma(z)$ . As follows from (57), the interfacial shape is determined by the interfacial tension distribution  $\sigma(z)$ , which is expected to be of the form sketched in Figure 10. Note that we have not used any conditions at  $z \rightarrow +\infty$  yet. Also, from (53b), we get the condition determining the function  $C_2(z)$ ,

$$C_2(z) = C_2^\infty \frac{\widehat{h}_\infty^2}{h^2} + \frac{\epsilon}{8} h \sigma_z, \quad (58)$$

as well as the general form of the stream-function in the thread region

$$\Psi = -\frac{w_\infty \widehat{h}_\infty^2}{2} \frac{\rho^2}{h^2} + \frac{\epsilon}{8} h \sigma_z \rho^2 \left(1 - \frac{\rho^2}{h^2}\right) + C_0, \quad (59)$$

and the  $z$ -component of the velocity field

$$w = w_\infty \frac{\widehat{h}_\infty^2}{h^2} + \frac{\epsilon}{4h} \sigma_z (2\rho^2 - h^2). \quad (60)$$

As one can observe from expressions (59) and (60), the flow consists of the self-similar solution (16), which has zero mass flux, superimposed with the constant flux solution, which is responsible for the mass flow through the thread—this mass flow rate  $Q_\infty$  is set by given experimental conditions and thus serves as a given parameter here (along with the cone semi-angle  $\theta^*$ , cf. Sec. II).

Now, let us look into the conditions at  $z \rightarrow +\infty$  necessary for matching the thread solution to the cone one. Since in the case when the solution approaches the cone,

$$h \rightarrow \frac{\tan \theta^*}{\epsilon} z, \quad \sigma \rightarrow \frac{\widetilde{\sigma}_{\min}}{z} \cos \theta^*, \quad (61)$$

Eq. (57) yields the condition

$$\epsilon c = \widetilde{\sigma}_{\min} \sin \theta^*; \quad (62)$$

the latter along with Eqs. (57) and (60) allow us to determine the interfacial velocity

$$w_s = w_\infty \left( \frac{\sigma}{\widehat{\sigma}_{\max}} \right)^2 + \frac{\epsilon c \sigma_z}{4 \sigma} = w_\infty \left( \frac{\sigma}{\widehat{\sigma}_{\max}} \right)^2 + \frac{\widetilde{\sigma}_{\min} \sin \theta^* \sigma_z}{4 \sigma}. \quad (63)$$

The interfacial velocity behaves at infinities as

$$\begin{aligned} z \rightarrow -\infty : w_s &\rightarrow w_\infty, \\ z \rightarrow +\infty : w_s &\rightarrow -\frac{\widetilde{\sigma}_{\min} \sin \theta^*}{4 z} + w_\infty \left( \frac{\widetilde{\sigma}_{\min}}{\widehat{\sigma}_{\max}} \right)^2 \frac{\cos^2 \theta^*}{z^2}, \end{aligned}$$

where we used the asymptotic behavior of  $h(z)$  and  $\sigma(z)$  for  $z \rightarrow \pm\infty$ . Note that the interfacial velocity  $w_s$  in the cone region decays to zero as  $z^{-1}$ , which is in accordance with the self-similar solution (29), while the flux responsible for the flow through the thread decays much faster in the cone region as  $z^{-2}$ , which can also be seen from mass conservation as applied to the thread and to the cone geometry, cf. Figure 7.

Note that the form of interfacial tension  $\sigma = (\widetilde{\sigma}_{\min}/z) \cos \theta^*$  suggests the natural scaling

$$z \rightarrow \widetilde{\sigma}_{\min} z, \quad (64)$$

which stretches the  $z$ -coordinate as is common for the ‘‘inner’’ solution in the matched asymptotic analysis<sup>21</sup> and consistent with the *a priori* considerations in Sec. IV A; here, the ‘‘outer’’ solution is the cone one. The fact that the lubrication equations solution (57) naturally captures the outer solution, i.e., conical shape, when  $\sigma \sim r^{-1}$ , is common in other problems: this property of the lubrication approximation is used to construct a composite solution *with the matching occurring internally*,<sup>54,55</sup> which is the procedure we will follow here. Thus, in order to keep both  $r$  and  $z$  coordinates on the same scale, will not rescale the  $z$ -coordinate.

Because  $\epsilon$  and  $c$  appear in the solution only as a product, without loss one can put  $c = \widehat{\sigma}_{\max}$  in (62) so that  $\widehat{h}_\infty = 1$  and the scaling for the thread radius becomes

$$\bar{h}_\infty = \epsilon l_c = \sin \theta^* \frac{\widetilde{\sigma}_{\min}}{\widehat{\sigma}_{\max}} l_c, \quad (65)$$

i.e., it is determined by the ratio of the values of interfacial tension in the cone and thread regions; the smaller the ratio  $\widetilde{\sigma}_{\min}/\widehat{\sigma}_{\max}$  the stronger the Marangoni effects. As follows from (65), the lower bound on the thread radius for a fixed cone semi-angle  $\theta^*$ ,

$$\inf \bar{h}_\infty = \sin \theta^* \frac{\sigma_{\min}}{\sigma_{\max}} l_c, \quad (66)$$

is determined by the ratio of the minimum and maximum interfacial tensions,  $\sigma_{\min}/\sigma_{\max}$ , which in turn are defined by a given material behavior  $\sigma(\gamma)$ . Since  $\widehat{h}_\infty = 1$  with the above choice of  $c$ , then instead of the mass flow rate  $Q_\infty = \pi \widehat{h}_\infty^2 w_\infty$  through the drop, we will utilize the escape velocity  $w_\infty$  in the thread.

The boundary-value problem for  $h(z)$  should be supplied with the surfactant transport Eq. (8) rewritten in cylindrical coordinates, which in the lubrication approximation (48) and non-dimensional form reads

$$\frac{d}{dz} (\gamma w_s) = \frac{1}{Pe_s} \frac{d^2 \gamma}{dz^2} + j_s. \quad (67)$$

Together with the expression for the interfacial velocity (63), in which  $\epsilon c$  was concluded to be equal to  $\widetilde{\sigma}_{\min} \sin \theta^*$  and the boundary conditions:

$$z \rightarrow z^* : \text{continuity of } h, h_z, \gamma, \gamma_z, \quad (68a)$$

$$z \rightarrow -\infty : h \rightarrow \widehat{h}_\infty, \frac{d\gamma}{dz} \rightarrow 0, \quad (68b)$$

it forms a complete boundary-value problem. In (68a),  $z^*$  is the point of matching between the thread and the cone solutions: this is analogous to the solution procedure in the Landau-Levich problem,<sup>25</sup>

where matching occurs at the point where the static meniscus is tangent to the thin film. Therefore, the problem reduces to the construction of the distribution  $\sigma(z)$  via solving the surfactant transport Eqs. (67) and (68) with a given material behavior  $\sigma(\gamma)$ . This in turn defines the interface shape (57) and the form of the stream-function (59)

$$\Psi = -\frac{w_\infty}{2} \left( \frac{\sigma}{\widehat{\sigma}_{\max}} \right)^2 \rho^2 + \frac{\widetilde{\sigma}_{\min} \sin \theta^*}{8} \frac{\sigma_z}{\sigma} \rho^2 \left( 1 - \rho^2 \frac{\sigma^2}{\widehat{\sigma}_{\max}^2} \right) + C_0, \quad (69)$$

and pressure found by integration of (55)

$$p = \widetilde{\sigma}_{\min} \sin \theta^* \left( \frac{\sigma}{\widehat{\sigma}_{\max}} \right)^2 + \text{const.} \quad (70)$$

Clearly, both forms of the stream-function and pressure resolve the singularity of (16) at  $r = 0$ . Also, as one can see from the expression for  $\Psi$ , it captures the flow structure with an internal stagnation point shown in Figure 7. With the choice  $C_0 = 0$ , the stream-function equals to zero at the interface, axis of symmetry, and along the surface inside the cone, which separates the fluid going into the thread and the one reversing back into the cone. This is the amazing property of the lubrication approximation, which starts from the assumption of a unidirectional flow and thus should be of parabolic character as the set of Eqs. (49) is, but is still capable of capturing the stagnation point as in Figure 7, which normally requires an elliptic operator to get resolved. This property of the lubrication approximations is known as weak ellipticity<sup>26</sup> and explains why lubrication approximations may apply well beyond the expected limits of their applicability.

Concluding these general theoretical considerations, it must be noted that:

- The Marangoni-driven tip-streaming exists even if only one phase is present and thus the limitation  $\mu_1/\mu_2 < 0.1$  from the externally driven tip-streaming does not apply here.
- While in this work we focused on the cone-shape singularities, as motivated by experiments,<sup>9</sup> the analysis suggests that the Marangoni-driven singularities may exhibit other interfacial shapes given by Eq. (57), which depend on the particularities of surfactant transport and equation of state  $\sigma(\gamma)$ .

Finally, note that the scaling law (65) is the leading order solution; the corrections to it can be found via the asymptotic procedure, which, as easy to demonstrate, provides corrections of the order of  $\epsilon^3$ :

$$\begin{aligned} h &= h_1 + \epsilon^3 h_3 + \dots, \\ p &= \epsilon p_1 + \epsilon^3 p_3 + \dots; \end{aligned}$$

however, this analysis is out of the scope of the present study.

### 3. Numerical integration

In order to integrate the lubrication Eq. (67) along with boundary conditions (68), it is important to note that Eq. (67) is Galilean invariant with respect to translation along the  $z$ -coordinate. Thus, when solving the boundary-value problem (67) and (68), one

1. fixes the values of  $w_\infty$  and  $\widehat{\gamma}_{\min}$ ;
2. integrates (67) up to the point where  $\gamma$  assumes the value  $\gamma^*$ ;
3. determines the location  $z^*$  of that point on the  $z$ -axis using the continuity of  $\gamma$

$$\gamma^* = d \left( \frac{z}{\cos \theta^*} \right)^\zeta \Rightarrow z^* = \left( \frac{\gamma^*}{d} \right)^{\frac{1}{\zeta}} \cos \theta^*; \text{ and} \quad (71)$$

4. varies  $\widehat{\gamma}_{\min}$  for a fixed  $w_\infty$  in order to match  $\gamma_z$  from the thread and cone regions

$$\left. \frac{d\gamma}{dz} \right|_{z^*} = \frac{d\zeta}{\cos \theta^*} \left( \frac{z^*}{\cos \theta^*} \right)^{\zeta-1}, \quad (72)$$

which gives the interfacial concentration  $\widehat{\gamma}_{\min}$  in the thread region. It is straightforward to show that continuity of  $h$  and  $h_z$  at  $z^*$  is automatically satisfied: this is due to the fact that conditions (61) were used to match the thread solution (57) to the cone one.

There are two key cases to consider depending on the value of the surfactant flux  $j_s$  to the interface due to chemical reaction: (1) when  $j_s = 0$  and thus the coefficient  $d$  in (36) is arbitrary, and (2) when  $j_s \neq 0$  and thus the coefficient  $d$  in (36) is determined by the surfactant flux to the interface. In the case  $j_s = 0$  and when diffusion is negligible,  $Pe_s \gg 1$ , the surfactant transport Eq. (67) reduces to  $d(\gamma w_s)/dz = 0$ , but its counterpart (34) in the cone region yields  $d\gamma/dz = 0$ , which is not compatible with the variation of interfacial tension (16). Despite being directly irrelevant to the present study, the corresponding solution is interesting in its own right and thus discussed in Appendix B.

Here we focus on the second case: note that due to the chosen system of coordinates  $d(\gamma w_s)/dz < 0$  and therefore  $j_s < 0$ , which makes the surfactant flux  $j_s$  to the interface consistent with the advection. For concreteness, the form of the surfactant flux is taken here as

$$j_s = b \gamma^\alpha (1 - \gamma)^\beta, \quad b < 0, \quad (73)$$

which is a standard approximation in other chemical reaction systems<sup>56</sup> allowing two equilibrium concentrations at the maximum,  $\gamma = \gamma_{\max} = 1$ , and minimum,  $\gamma = \gamma_{\min} = 0$ , values of  $\gamma$ . Note that this law reduces to the power-law approximation (37) of  $j_s$  in the cone region as when  $z \rightarrow +\infty$ ,  $j_s \sim b \gamma^\alpha$  with  $\alpha = 1 - 2/\zeta$ ; accuracy of such an approximation becomes better if  $\alpha \gg \beta$ .

The boundary condition for the surfactant concentration  $d\gamma/dz \rightarrow 0$  as  $z \rightarrow -\infty$  deserves a few comments. From experiments,<sup>9</sup> it is known that the emitted droplets carry surfactant, which can be due to two factors: the surfactant is supplied by advection from the cone region—indeed  $\widehat{\gamma}_{\min} \neq 0$ —and by a chemical reaction happening at the droplet interface, i.e., the surfactant is produced after the droplets detach from the thread. This resolves the paradox formulated in Sec. IB: small emitted droplets indeed end up having low interfacial tension due to the above mechanisms.

It is remarkable that the two-point boundary-value problem (67) and (68) with (57) and composite  $\sigma(\gamma)$  given by (38) and (39) yield a solution even without a diffusion term. Even though the resulting equation for  $\gamma$  appear to be first-order, the form of  $w_s$  given by (63) shows that the advection term in (67) is second order in the  $z$ -derivative; this is one of the sources of the weak ellipticity property of the lubrication equations. The role of diffusion, however, is to further smooth out the profile of  $\gamma(z)$ .

Example computations are shown in Figures 11 and 12. One way to interpret Figure 11 is that given a mass flux  $w_\infty$ , one gets a certain value of  $\widehat{\gamma}_{\min}$  in the thread, which defines the solution structure everywhere as shown in Figure 12. For larger flow rates  $w_\infty$ , one may get two different solutions  $\widehat{\gamma}_{\min}$ , which physically means that either one of them is unstable or there is a hysteresis phenomenon. As pointed out in Sec. IV B 2, the constructed solution captures the whole “cone + thread” region with the matching occurring internally as can be seen from Figure 12. The self-similar and slender-jet solutions have an overlapping region of validity in the neighborhood of the point  $z^*$ , where the linear (38) and power-law (39) forms of the composite material behavior match along with their first order derivatives  $d\sigma/d\gamma$ .

Recalling all the scalings performed in order to arrive at the lubrication approximation, the dimensional thread thickness is given by (65), which has the lower bound (66). Since the interfacial tensions in the clean and surfactant interface case differ by two orders of magnitude,<sup>10</sup> formulas (65) and (66) give the right estimate for the experimentally observed difference between the drop size  $\sim 0.5$  mm, which is of the order of the capillary length  $l_c$ , and the thread diameter  $\sim 0.5$   $\mu$ m. Dependence of the factor  $\widetilde{\sigma}_{\min}/\widetilde{\sigma}_{\max}$  on  $\widehat{\gamma}_{\min}$  is shown in Figure 11(b) for  $d = 1$ : as mentioned earlier, the factor  $\widetilde{\sigma}_{\min}/\widetilde{\sigma}_{\max}$  determining the thread radius (65) scales with  $d$  as  $\sim d^{-1/\zeta}$  and thus the larger the magnitude of  $d$ , the smaller the value of this factor. In view of well-posedness of the problem, i.e., not high sensitivity to the slight variation in the coefficients (in particular, the form of the equation of state), the use of an empirical state equation instead of (38) and (39) will not change the qualitative behavior of the constructed solutions.

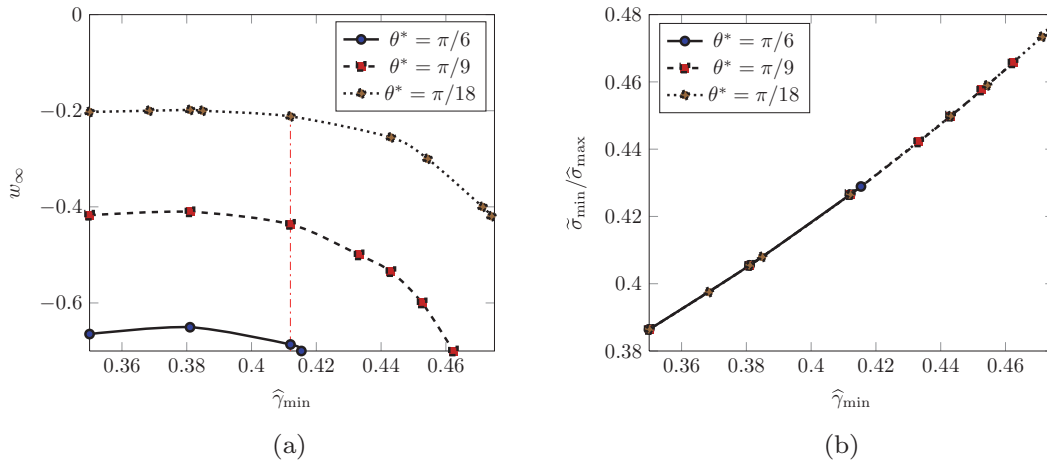


FIG. 11. (Color online) Sample solution to the boundary-value problem (67) and (68) with (57) and composite  $\sigma(\gamma)$  given by (38) and (39): (a) functional dependence  $w_\infty(\widehat{\gamma}_{\min})$ ; vertical dash-dotted line corresponds to the profiles of  $\gamma(z)$ ,  $\sigma(z)$ , and  $h(z)$  given in Figure 12, (b) functional dependence of  $\widehat{\sigma}_{\min}/\widehat{\sigma}_{\max}$  on  $\widehat{\gamma}_{\min}$  shown for  $d = 1$ ; note that each  $\widehat{\gamma}_{\min}$  for a given  $\theta^*$  has a value of  $w_\infty$  associated with it according to Figure 11(a). Marks are computed points, and lines are interpolations between them.

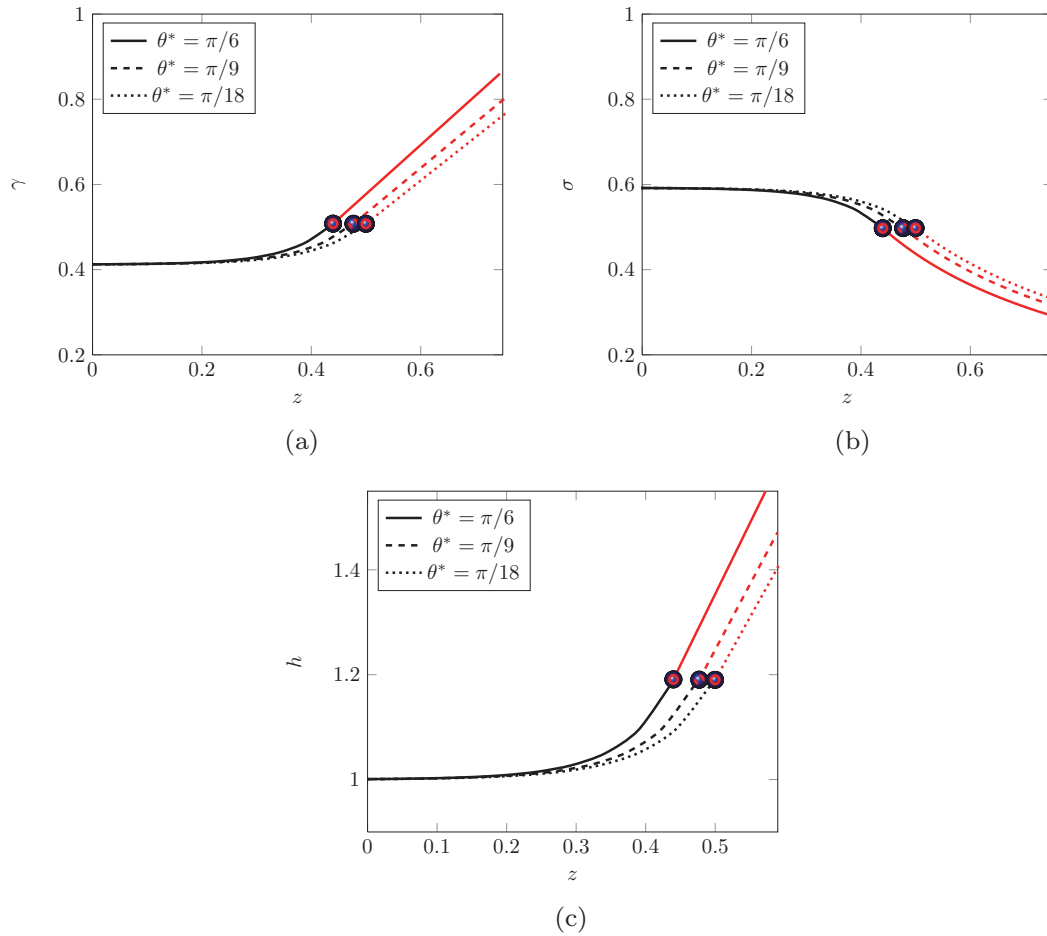


FIG. 12. (Color online) Result of integration of (67) and (68) for  $\widehat{\gamma}_{\min} = 0.412$  and different  $\theta^*$  corresponding to the vertical dash-dotted line in Figure 11: profiles of (a)  $\gamma(z)$ , (b)  $\sigma(z)$ , (c)  $h(z)$ . Dots on the plots indicate the point of matching between the thread and the cone solutions. Note that the  $z$ -coordinate corresponds to the true one—the cone profile meets the origin of the  $z$ -coordinate.

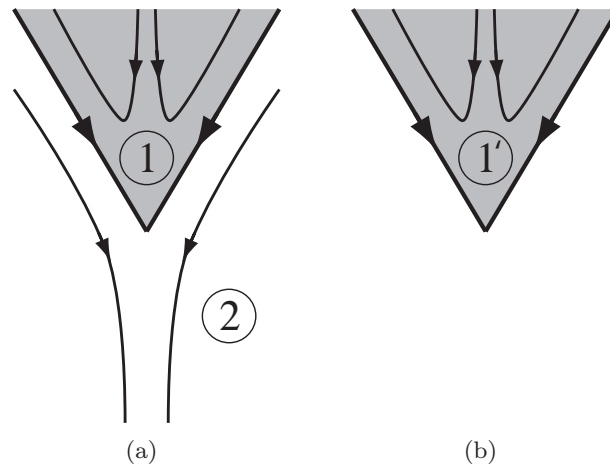


FIG. 13. On the equivalence of one- and two-phase motions: (a) two-phase system, (b) equivalent one-phase system.

## V. CONCLUSIONS

In this work, an analytical study of steady Marangoni-driven singularities is presented in the axisymmetric three-dimensional case. The study involved finding a family of self-similar solutions in the neighborhood of a singularity as well as the resolution of this singularity via the construction of a thread solution based on a singular perturbation technique and matching to the self-similar solution. The scaling law for the thread radius (65) and (66) is determined, which demonstrates the dependence on the lowest,  $\tilde{\sigma}_{\min}$ , and highest,  $\tilde{\sigma}_{\max}$ , values of the interfacial tension, the cone semi-angle  $\theta^*$ , and the material behavior  $\sigma(\gamma)$ . While the analysis is done in the context of surfactant Marangoni-driven singularities, the obtained results and conclusions are general and independent of the nature of the Marangoni stresses. However, one has yet to discover experimentally interfacial singularities driven by temperature and electric field gradients. Also, it must be noted that even though this work is motivated by experiments of Fernandez and Homsy,<sup>9</sup> further careful experimental studies are needed to uncover the physics of the observed tip-streaming phenomena.<sup>9</sup>

While in this work we focused on the cone-shape singularities, as motivated by experiments,<sup>9</sup> the analysis suggests that the Marangoni-driven singularities may exhibit other interfacial shapes given by Eq. (57), which depend on the particularities of surfactant transport and equation of state  $\sigma(\gamma)$ . Although we considered only one class of self-similar solutions (16) corresponding to  $n = 1$  and resolution of this singularity at the tip, similar analysis can be conducted for higher order solutions,  $n > 1$ . All the constructed shapes here are steady, so future studies are required to analyze their stability with respect to unsteady perturbation: while the thread is clearly unstable via Rayleigh-Plateau mechanism, the drop may experience other instabilities for certain range of parameters, e.g., for certain mass flow rates. Also, among the unanswered theoretical questions is the one on the physical mechanisms responsible for the transition between “thread” and “no-thread” regimes. At the methodological level, it would be useful for this and similar problems to develop a systematic singular domain perturbation techniques capable of perturbing singular base state solutions, such as the self-similar solutions with the conical symmetry constructed here.

## ACKNOWLEDGMENTS

This work was partially supported by the National Science Foundation (NSF) CAREER award under Grant No. 1054267. The author is grateful to Professor Bud Homsy for reading over the paper and providing useful feedback.

## APPENDIX A: ON EQUIVALENCE OF ONE- AND TWO-PHASE MOTIONS

In this section, we prove the Principle of equivalence of one- and two phase creeping flow motions, given by Proposition 1. Given a steady-state system of two immiscible viscous phases separated by an interface, such that only one phase contains singularities, can one replace it with an equivalent one-phase system which has the same steady-state evolution of the interface? What would be the connection of the velocity and pressure fields between the new and old systems?

*Proof.* For concreteness, let us consider the first phase occupying region  $D_1 \in \mathbb{R}^2$ , while the second phase occupies its complement  $D_2 = \mathbb{R}^2/D_1$ , cf. Figure 13(a), and the interface between them is designated by  $\Gamma$ , which can be given in an implicit form  $F(\mathbf{x}) = 0$ . The same arguments apply to the axisymmetric case in  $\mathbb{R}^3$ . The reason to consider the case when only one phase has singularities (e.g., sink, source, dipole, vortex dipole) is because in general one cannot capture the physics correctly by replacing the phase with a singularity by an inviscid inertialess phase.

Let us also denote the properties of the first phase (possibly with a singularity) by  $\mu_1, \rho_1, \psi_1$ , and  $p_1$  (viscosity, density, stream-function, and pressure, respectively), while the other phase is characterized by  $\mu_2, \rho_2, \psi_2$ , and  $p_2$ . The goal is to replace this system with a new one, cf. Figure 13(b), when phase 2 is described by new properties  $\mu'_2 = 0, \rho'_2 = 0, \psi'_2 = 0$ , and  $p'_2 = 0$ , while the properties of phase 1, i.e.,  $\mu'_1, \rho'_1, \psi'_1$ , and  $p'_1$ , need to be determined *under the condition that the interface evolution stays intact, in particular, the interfacial velocity should stay the same.*

The bulk dynamics is governed by the Stokes equations

$$\Delta^2 \psi_1 = 0 \text{ for } \mathbf{x} \in D_1, \quad \Delta^2 \psi_2 = 0 \text{ for } \mathbf{x} \in D_2,$$

while interface dynamics obeys the no-slip  $\mathbf{u}^{(1)} = \mathbf{u}^{(2)}$ , the dynamic normal and tangential, and kinematic conditions

$$[\mathbf{n} \cdot \mathbf{T} \cdot \mathbf{n}]_1^2 = \sigma \nabla \cdot \mathbf{n},$$

$$[\mathbf{t} \cdot \mathbf{T} \cdot \mathbf{n}]_1^2 = -\mathbf{t} \nabla_s \sigma,$$

$$\nabla F \cdot \mathbf{u}^{(i)} = 0,$$

respectively. Here we naturally consider the case when viscosities of these two phases are not necessarily equal; thus, to preserve the structure and signs in the dynamic interfacial conditions when we transform to a single phase, let us introduce new phase velocity  $\mathbf{u}'$  and pressure  $p'$  according to

$$\mu' \mathbf{u}' = \mu_1 \mathbf{u}^{(1)} - \mu_2 \mathbf{u}^{(2)}, \quad p' = p_1 - p_2,$$

so that the new viscous stress tensor becomes  $\mu' \mathbf{e}' = \mu_1 \mathbf{e}^{(1)} - \mu_2 \mathbf{e}^{(2)}$  and thus the complete stress tensor is  $\mathbf{T}' = \mathbf{T}^{(1)} - \mathbf{T}^{(2)}$ , which leaves the signs in the dynamic interfacial conditions unchanged and thus makes the dynamic conditions to be stated as if there is only one phase (primed variables)

$$\mathbf{n} \cdot \mathbf{T}' \cdot \mathbf{n} = -\sigma \nabla \cdot \mathbf{n}, \tag{A1a}$$

$$\mathbf{t} \cdot \mathbf{T}' \cdot \mathbf{n} = \mathbf{t} \nabla_s \sigma. \tag{A1b}$$

The interfacial velocity of this new phase is then given by (recall the continuity of the velocity field across the interface,  $\mathbf{u}^{(1)} = \mathbf{u}^{(2)}$ )

$$\mathbf{u}' = \frac{\mu_1 - \mu_2}{\mu'} \mathbf{u}^{(1)},$$

i.e., the kinematic boundary condition,  $\nabla F \cdot \mathbf{u}' = 0$ , is satisfied as well. The no-slip condition at the interface is redundant now. Next, because of the linearity of the bulk dynamics, it is enough to solve for the bulk dynamics of the new phase only,  $\Delta^2 \psi' = 0$ , where  $\mathbf{u}' = \nabla \times \psi'$ ,  $\psi' = (0, 0, \psi')$ ; this makes the problem for an effective phase closed. In order to preserve the magnitude and direction of the interfacial velocity, one should choose  $\mu' = \mu_2 - \mu_1$ . Note that if  $\mu_2 > \mu_1$ , then one needs to change the sign of  $\sigma$  in (A1) in order to preserve the form of the dynamic interfacial condition,

which corresponds effectively to negative interfacial tension. From these considerations, one also concludes that in the case  $\mu_1 = \mu_2$  it is impossible to replace a two-phase system with one phase having the interfacial velocity, which is the same as in the original two-phase system.

The above simple arguments prove that indeed one can replace a two-phase system with an equivalent one phase, under the conditions that the singularities are present only in one phase and viscosities of the phases are not equal, and therefore conduct the analysis for an equivalent one-phase system.  $\square$

## APPENDIX B: THREAD SOLUTION WITHOUT CHEMICAL REACTION

In the case when there is no surfactant production at the interface,  $j_s = 0$ , and diffusion is negligible,  $Pe_s \gg 1$ , the surfactant transport Eq. (67) can be integrated to produce

$$\gamma w_s = \widehat{\gamma}_{\min} w_\infty, \quad (\text{B1})$$

which implies that surfactant is feeded along the circumference of the base of a finite drop and then transported to the thread. The conservation law (B1) gives the evolution equation for  $\gamma$ ,

$$\frac{d\gamma}{dz} = \frac{4 w_\infty \sigma}{\sin \theta^* \widetilde{\sigma}_{\min}} \frac{I}{d\sigma/d\gamma}, \quad I = \frac{\widehat{\gamma}_{\min}}{\gamma} - \frac{\sigma^2}{\widehat{\sigma}_{\max}^2}. \quad (\text{B2})$$

Clearly, in order to get interfacial concentration growing monotonically from its value  $\widehat{\gamma}_{\min}$  in the thread to  $\widetilde{\gamma}_{\max}$  in the cone (cf. Figure 10) necessary for a Marangoni flow maintaining the steady solution, the expression  $I$  should be greater or equal to zero. With the linear equation of state (38), which we apply in the thread region, this implies that

$$\begin{aligned} \left. \frac{dI}{d\gamma} \right|_{\widehat{\gamma}_{\min}} \geq 0 &\Rightarrow \widehat{\gamma}_{\min} \geq \frac{\sigma_{\max}(\sigma_{\max} - \sigma_{\min})}{2 + (\sigma_{\max} - \sigma_{\min})} \\ &\simeq \frac{\sigma_{\max}^2}{2 + \sigma_{\max}} \simeq \frac{1}{3}, \end{aligned} \quad (\text{B3})$$

provided  $\sigma_{\min} \ll \sigma_{\max} = 1$ . It is notable that due to  $\frac{d\gamma}{dz}|_{z^*} \sim d^{1/\zeta}$  and  $\widetilde{\sigma}_{\min} \sim d^{-1/\zeta}$ , the functional relation  $F(\theta^*, w_\infty, \widehat{\gamma}_{\min}) = 0$  between  $\theta^*$ ,  $w_\infty$ , and  $\widehat{\gamma}_{\min}$ , determined from the solution to the boundary-value problem (67) and (68), does not depend on the value of  $d$ , as can be seen from equation (B2). However, the resulting profiles  $h(z)$ ,  $\gamma(z)$ , and  $\sigma(z)$  do depend on the values of  $d$ . The factor  $\widetilde{\sigma}_{\min}/\widehat{\sigma}_{\max}$  determining the thread radius (65) scales with  $d$  as  $\sim d^{-1/\zeta}$  and thus the larger the magnitude of  $d$ , the smaller the value of this factor and thus the sharper the singularity. Also, this factor  $\widetilde{\sigma}_{\min}/\widehat{\sigma}_{\max}$  does not depend on the cone semi-angle  $\theta^*$  due to the fact that for fixed  $\widehat{\gamma}_{\min}$  and  $\widetilde{\gamma}_{\max}$  (or  $\widetilde{\sigma}_{\min}$ , which is independent of  $\theta^*$ ), one has a fixed thread radius (65) and thus the mass flux  $w_\infty$  should scale as  $\tan \theta^*$ , as can be seen from Eq. (B2).

- <sup>1</sup> R. Krechetnikov, "Marangoni-driven singularities via mean-curvature flow," *J. Phys. A* **43**, 242001 (2010).
- <sup>2</sup> G. L. van der Mensbrugghe, "Sur la tension superficielle des liquides considérée au point de vue de certains mouvements observés à leur surface," *Mémoires Couronnés (et autres) de l'Académie Royale des Sciences etc de Bruxelles* **34**, 1 (1869).
- <sup>3</sup> L. Rayleigh, "Measurements of the amount of oil necessary in order to check the motions of camphor upon water," *Proc. R. Soc. London* **47**, 364 (1890).
- <sup>4</sup> F. H. Garner, C. W. Nutt, and M. F. Mohtadi, "Pulsation and mass transfer of pendent liquid droplets," *Nature (London)* **175**, 603 (1955).
- <sup>5</sup> D. A. Haydon, "Oscillating droplets and spontaneous emulsification," *Nature (London)* **176**, 839 (1955).
- <sup>6</sup> J. B. Lewis, "Liquid-liquid extraction. The extraction of uranyl nitrate in a wetted wall column," *Trans. Inst. Chem. Eng.* **31**, 323 (1953).
- <sup>7</sup> K. Sigwart and H. Nasselstein, "The mechanism of material transfer through the boundaries of two liquid phases," *Z. Ver. Dtsch. Ing.* **98**, 453 (1956).
- <sup>8</sup> M. v. Stackelberg, E. Klockner, and P. Mohrhauer, "Spontane Emulgierung infolge negativer Grenzflächenspannung," *Kolloidschr* **115**, 53 (1949).
- <sup>9</sup> J. M. Fernandez and G. M. Homsy, "Chemical reaction-driven tip-streaming phenomena in a pendant drop," *Phys. Fluids* **16**, 2548 (2004).
- <sup>10</sup> R. Krechetnikov and G. M. Homsy, "On physical mechanisms in chemical reaction-driven tip-streaming," *Phys. Fluids* **16**, 2556 (2004).

- <sup>11</sup> W. W. Mansfield, "The spontaneous emulsification of mixtures of oleic acid and paraffin oil in alkaline solutions," *Aust. J. Sci. Res., Ser. A* **5**, 331 (1952).
- <sup>12</sup> G. I. Taylor, "The formation of emulsions in definable fields of flow," *Proc. R. Soc. London, Ser. A* **146**, 501 (1934).
- <sup>13</sup> H. A. Stone, "Dynamics of drop deformation and breakup in viscous fluids," *Annu. Rev. Fluid Mech.* **26**, 65 (1994).
- <sup>14</sup> R. A. de Bruijn, "Tipstreaming of drops in simple shear flows," *Chem. Eng. Sci.* **48**, 277 (1993).
- <sup>15</sup> M. Siegel, "Influence of surfactant on rounded and pointed bubbles in two-dimensional Stokes flow," *SIAM J. Appl. Math.* **59**, 1998 (1999).
- <sup>16</sup> Y. T. Hu, D. J. Pine, and L. G. Leal, "Drop deformation, breakup, and coalescence with compatibilizer," *Phys. Fluids* **12**, 484 (2000).
- <sup>17</sup> A. Acrivos and T. S. Lo, "Deformation and breakup of a single slender drop in an extensional flow," *J. Fluid Mech.* **86**, 641 (1978).
- <sup>18</sup> C. D. Eggleton, Y. P. Pawar, and K. J. Stebe, "Insoluble surfactants on a drop in an extensional flow: A generalization of the stagnated surface limit to deforming interfaces," *J. Fluid Mech.* **385**, 79 (1999).
- <sup>19</sup> C. D. Eggleton, T.-M. Tsai, and K. J. Stebe, "Tip streaming from a drop in the presence of surfactants," *Phys. Rev. Lett.* **87**, 048302 (2001).
- <sup>20</sup> S. L. Anna and H. C. Mayer, "Microscale tipstreaming in a microfluidic flow focusing device," *Phys. Fluids* **18**, 121512 (2006).
- <sup>21</sup> M. D. V. Dyke, *Perturbation Methods in Fluid Mechanics* (Parabolic, Stanford, CA, 1975).
- <sup>22</sup> D. Henry, *Perturbation of the Boundary in Boundary-Value Problems of Partial Differential Equations* (Cambridge University Press, New York, 2005).
- <sup>23</sup> D. D. Joseph and R. L. Fosdick, "The free surface on a liquid between cylinders rotating at different speeds," *Arch. Ration. Mech. Anal.* **49**, 321 (1972).
- <sup>24</sup> M. C. Sostarecz and A. Belmonte, "Motion and shape of a viscoelastic drop falling through a viscous fluid," *J. Fluid Mech.* **497**, 235 (2003).
- <sup>25</sup> L. Landau and B. Levich, "Dragging of a liquid by a moving plate," *Acta Physicochim. USSR* **17**, 42 (1942).
- <sup>26</sup> R. Krechetnikov, "On application of lubrication approximations to nonunidirectional coating flows with clean and surfactant interfaces," *Phys. Fluids* **22**, 092102 (2010).
- <sup>27</sup> A. T. Layton, "An efficient numerical method for the two-fluid Stokes equations with a moving immersed boundary," *Comput. Methods Appl. Mech. Eng.* **197**, 2147 (2008).
- <sup>28</sup> D. Jones, "Superficial complexity," *Nature (London)* **400**, 719 (1999).
- <sup>29</sup> F. J. Higuera, "Flow rate and electric current emitted by a Taylor cone," *J. Fluid Mech.* **484**, 303 (2003).
- <sup>30</sup> L. T. Cherney, "Structure of Taylor cone-jets: Limit of low flow rates," *J. Fluid Mech.* **378**, 167 (1999).
- <sup>31</sup> G. I. Taylor, "Disintegration of water drops in an electric field," *Proc. R. Soc. London, Ser. A* **280**, 383 (1964).
- <sup>32</sup> G. I. Taylor, "Conical free surfaces and fluid interfaces," in *Proceedings of the 11th International Congress of Applied Mathematics, Munich*, edited by G. K. Batchelor (Springer, Heidelberg, 1964), pp. 191–219.
- <sup>33</sup> L. Hayati, A. I. Bailey, and T. F. Tadros, "Mechanism of stable jet formation in electrohydrodynamic atomization," *Nature (London)* **319**, 41 (1986).
- <sup>34</sup> C. I. Chivetelu, V. Hornof, and G. H. Neale, "Interaction of aqueous caustic with acidic oils," *J. Can. Pet. Technol.* **28**, 71 (1989).
- <sup>35</sup> J. Happel and H. Brenner, *Low Reynolds Number Hydrodynamics* (Prentice-Hall, Englewood Cliffs, NJ, 1965).
- <sup>36</sup> L. D. Landau and E. M. Lifshitz, *Fluid Mechanics* (Pergamon, New York, 1989).
- <sup>37</sup> C.-S. Yih, F. Wu, A. K. Garg, and S. Leibovich, "Conical vortices: a class of exact solutions of the Navier-Stokes equations," *Phys. Fluids* **25**, 2147 (1982).
- <sup>38</sup> A. Barrero, A. M. Gañán-Calvo, J. Dávila, A. Palacio, and E. Gómez-González, "Low and high Reynolds number flows inside Taylor cones," *Phys. Rev. E* **58**, 7309 (1998).
- <sup>39</sup> A. Barrero, A. M. Gañán-Calvo, J. Dávila, A. Palacio, and E. Gómez-González, "The role of the electrical conductivity and viscosity on the motions inside Taylor cones," *J. Electrostat.* **47**, 13 (1999).
- <sup>40</sup> L. I. Sedov, *Similarity and Dimensional Methods in Mechanics* (Academic, New York, 1961).
- <sup>41</sup> G. I. Barenblatt, *Scaling, Self-Similarity, and Intermediate Asymptotics* (Cambridge University Press, New York, 1996).
- <sup>42</sup> G. B. Folland, *Introduction to Partial Differential Equations* (Princeton University, Princeton, NJ, 1995).
- <sup>43</sup> R. J. Adler, M. J. Bazin, and M. Schiffer, *Introduction to General Relativity* (McGraw-Hill, New York, 1975).
- <sup>44</sup> Y. H. Kim and D. T. Wasan, "Dynamic surface tension of ionic surfactant solution," *J. Ind. Eng. Chem.* **3**, 119 (1997).
- <sup>45</sup> C.-H. Chang and E. I. Franses, "Adsorption dynamics of surfactants at the air/water interface: A critical review of mathematical models, data, and mechanisms," *Colloids Surf., A* **100**, 1 (1995).
- <sup>46</sup> E. H. Lucassen-Reynders, "Surface equation of state for ionized surfactants," *J. Phys. Chem.* **70**, 1777 (1966).
- <sup>47</sup> S.-Y. Lin, Y.-C. Lee, M.-W. Yang, and H.-S. Liu, "Surface equation of state of nonionic Cmc surfactants," *Langmuir* **19**, 3164 (2003).
- <sup>48</sup> Besides the fact that  $\sigma \rightarrow -\infty$  as  $\gamma \rightarrow \gamma_\infty$ , let us do a simple calculation for the Frumkin equation applied to sodium dodecyl sulfate

$$\sigma = \sigma_{\max} + nRT\gamma_\infty \ln\left(1 - \frac{\gamma}{\gamma_\infty}\right),$$

where  $\gamma_\infty = 10^{-5} \text{ mol} \cdot \text{m}^{-2}$  is the maximum surface concentration,  $T = 298 \text{ K}$ ,  $R = 8.3145 \text{ J}/(\text{mol} \cdot \text{K})$  the gas constant,  $\sigma_{\max} = 72 \text{ mN/m}$  the clean interface tension, and  $n = 2$  for non-ionic surfactants. Based on this equation, the value of the interfacial tension at  $\gamma = 3 \cdot 10^{-6} \text{ mol} \cdot \text{m}^{-2}$ , which corresponds to CMC, is  $\sigma = 54.3 \text{ mN/m}$ , which is substantially

higher than the true value  $\sigma \simeq 38$  mN/m. Therefore, one cannot rely on Frumkin's equation for the whole range of concentrations below CMC.

- <sup>49</sup> A. Sheludko, "Thin liquid films," *Adv. Colloid Interface Sci.* **1**, 391 (1967).
- <sup>50</sup> D. A. Edwards, H. Brenner, and D. T. Wasan, *Interfacial Transport Processes and Rheology* (Butterworth-Heinemann, Boston, MA, 1991).
- <sup>51</sup> B. D. Edmonstone, R. V. Craster, and O. K. Matar, "Surfactant-induced fingering phenomena beyond the critical micelle concentration," *J. Fluid Mech.* **564**, 105 (2006).
- <sup>52</sup> J. M. Fernandez and G. M. Homsy, "Viscous fingering with chemical reaction: Effect of *in situ* production of surfactants," *J. Fluid Mech.* **480**, 267 (2003).
- <sup>53</sup> Y. Touhami, V. Hornof, and G. H. Neale, "Dynamic interfacial tension behavior of acidified oil/surfactant enhanced alkaline systems – I. Experimental studies," *Colloids Surf., A* **132**, 61 (1998).
- <sup>54</sup> S. D. R. Wilson, "The drag-out problem in film coating theory," *J. Eng. Math.* **1982**, 209 (1982).
- <sup>55</sup> J. Ratulowski and H.-C. Chang, "Marangoni effects of trace impurities on the motion of long gas bubbles in capillaries," *J. Fluid Mech.* **210**, 303 (1990).
- <sup>56</sup> A. de Witt and G. M. Homsy, "Viscous fingering in reaction-diffusion systems," *J. Chem. Phys.* **110**, 8663 (1999).